

Melt Inclusions in Olivine Phenocrysts: Using Diffusive Re-equilibration to Determine the Cooling History of a Crystal, with Implications for the Origin of Olivine-phyric Volcanic Rocks

LEONID V. DANYUSHEVSKY^{1*}, SERGUEI SOKOLOV² AND TREVOR J. FALLOON¹

¹SCHOOL OF EARTH SCIENCES AND CENTRE FOR ORE DEPOSIT RESEARCH, UNIVERSITY OF TASMANIA, GPO BOX 252-79, HOBART, TAS. 7001, AUSTRALIA

²CSIRO DIVISION OF MARINE RESEARCH, GPO BOX 1538, HOBART, TAS. 7001, AUSTRALIA

RECEIVED JUNE 30, 2001; REVISED TYPESCRIPT ACCEPTED MARCH 6, 2002

A technique is described for determining the cooling history of olivine phenocrysts. The technique is based on the analysis of the diffusive re-equilibration of melt inclusions trapped by olivine phenocrysts during crystallization. The mechanism of re-equilibration involves diffusion of Fe from and Mg into the initial volume of the inclusion. The technique applies to a single crystal, and thus the cooling history of different phenocrysts in a single erupted magma can be established. We show that melt inclusions in high-Fo olivine phenocrysts from mantle-derived magmas are typically partially re-equilibrated with their hosts at temperatures below trapping. Our analysis demonstrates that at a reasonable combination of factors such as (1) cooling interval before eruption (<350°C), (2) eruption temperatures (>1000°C), and (3) inclusion size (<70 µm in radius), partial re-equilibration of up to 85% occurs within 3–5 months, corresponding to cooling rates faster than 1–2°/day. Short residence times of high-Fo phenocrysts suggest that if eruption does not happen within a few months after a primitive magma begins cooling and crystallization, olivines that crystallize from it are unlikely to be erupted as phenocrysts. This can be explained by efficient separation of olivine crystals from the melt, and their rapid incorporation into the cumulate layer of the chamber. These results also suggest that in most cases erupted high-Fo olivine phenocrysts retain their original composition, and thus compositions of melt inclusions in erupted high-Fo olivine phenocrysts do not suffer

changes that cannot be reversed. Short residence times also imply that large unzoned cores of high-Fo phenocrysts cannot reflect diffusive re-equilibration of originally zoned phenocrysts. The unzoned cores are a result of fast efficient accumulation of olivines from the crystallizing magma, i.e. olivines are separated from the magma faster than melt changes its composition. Thus, the main source of high-Fo crystals in the erupted magmas is the cumulate layers of the magmatic system. In other words, olivine-phyric rocks represent mixtures of an evolved transporting magma (which forms the groundmass of the rock) with crystals that were formed during crystallization of more primitive melt(s). Unlike high-Fo olivine phenocrysts, the evolved magma may reside in the magmatic system for a long time. This reconciles long magma residence times estimated from the compositions of rocks with short residence times of high-Fo olivine phenocrysts.

KEY WORDS: melt inclusions; olivine; picrites; residence time; diffusion

INTRODUCTION

Timing magma crystallization and cooling is an important geological problem. Significant efforts have therefore

*Corresponding author. Telephone: +61-3-62262429. Fax: +61-3-62232547. E-mail: l.dan@utas.edu.au

been directed at estimating the residence time of magmas in magma chambers. Previous studies have used a variety of approaches including radiogenic isotope decay-series disequilibria (e.g. Volpe & Hammond, 1991; Pyle, 1992; Sigmarsson, 1996; Hawkesworth *et al.*, 2000); geochemical fluctuations in volcanic series (Albarède, 1993); diffusion rates in crystals and melts (e.g. Christensen & DePaolo, 1993; Francalanci *et al.*, 1999; Zellmer *et al.*, 1999); and crystal size distribution in erupted lavas (e.g. Mangan, 1990). The resulting estimates of magma residence time vary from ten years to hundreds of thousands of years [see Hawkesworth *et al.* (2000) for a recent summary].

Relatively little is known about the residence times of individual olivine phenocrysts that have crystallized from primitive mantle-derived magmas. Nakamura (1995) studied compositional zoning of magnesian (high-Fo) olivine phenocrysts from two Japanese volcanoes and estimated their residence times to be of the order of several months, i.e. significantly shorter than estimates of magma residence times.

In this paper we describe a new technique for determining the cooling history of olivine phenocrysts, based on the analysis of the diffusive re-equilibration of melt inclusions trapped by olivine phenocrysts. The technique can be used for estimating the cooling history of olivine phenocrysts between temperatures of their crystallization and diffusion closure. The technique applies to a single crystal, and thus the cooling history of different phenocrysts in a single erupted magma can be established. Using a number of magmatic suites from different tectonic settings, we demonstrate that high-Fo olivine phenocrysts generally spend a short time at temperatures below their crystallization temperature, confirming the results of Nakamura (1995). We also discuss some implications of our results for the origin of high-Fo olivine-phyric volcanic rocks.

METHOD

Re-equilibration of Fe and Mg between melt inclusions and their host olivine phenocrysts has been described in detail by Danyushevsky *et al.* (2000), with the main points summarized briefly below. The underlying assumption of this model is that the composition of the host olivine does not change after trapping of the inclusion (throughout this paper we will refer to a melt inclusion as simply the 'inclusion').

Cooling of an inclusion after trapping results in crystallization of olivine from the trapped melt, forming an olivine rim on the walls of the inclusion (Fig. 1). The crystallizing olivine rim is progressively enriched in Fe and depleted in Mg, i.e. has lower proportion of the forsterite component (Fo), resulting in a compositional

gradient within the rim. The existence of this compositional gradient causes re-equilibration of the inclusion with its host. This re-equilibration is achieved by diffusion of Fe out of, and Mg into the initial volume of the inclusion. This leads to a rapid decrease in Fe content of the residual melt inside the inclusion, a process referred to as 'Fe-loss' by Danyushevsky *et al.* (2000). The extent of Fe-loss, i.e. the degree of re-equilibration, is defined as the amount of FeO* 'lost' by the residual melt relative to the amount that is 'lost' in the case of complete re-equilibration.

Known values of the diffusion coefficient for Fe–Mg inter-diffusion ($D_{\text{Fe-Mg}}$) in olivine (e.g. Chakraborty, 1997) allow calculation of time required for re-equilibration to occur. If an inclusion is completely re-equilibrated, it is possible to calculate the minimum time that the host phenocrysts spent at temperatures between trapping and diffusion closure. However, if re-equilibration is not complete when the closure temperature is reached and a diffusion profile around an inclusion is preserved, a quantitative time estimate can be made.

It should be noted that this technique does not allow an estimate of the residence time at (or close to) the trapping temperature, because at these conditions there is no crystallization within the inclusion.

We will first consider a case of instant cooling (Fig. 1a). In this case the zoned rim grows first and then re-equilibration occurs while a grain resides at the lower end of the cooling interval. For this case we will examine the effects on re-equilibration time of: (1) inclusion size; (2) residence temperature; (3) cooling interval; (4) melt composition (see caption to Fig. 1a for definitions). Models of diffusion and olivine–melt equilibria, and modelling of olivine fractionation inside inclusions have been described in detail by Danyushevsky *et al.* (2000) [note that there is a printing error in the model description in Danyushevsky *et al.* (2000): the flux of FeO* from the in-

clusion to the host should be $D \frac{\delta C}{\delta r} \Big|_{r=r_0}$]. When modelling

olivine fractionation inside inclusions, we have assumed that inclusions behave as closed systems for oxygen, and thus Fe³⁺ behaves as an incompatible element, i.e. its concentration simply increases during crystallization [see Danyushevsky *et al.* (2000) for more details].

The second case we will consider is when re-equilibration and cooling occur simultaneously (Fig. 1b). For this case we will examine the effect of cooling rate on re-equilibration time at given cooling interval and trapping temperature.

Effects of the cooling interval and inclusion size on re-equilibration time

The trapped inclusion composition (Table 1, No. 1) used in calculations presented in this section is an anhydrous

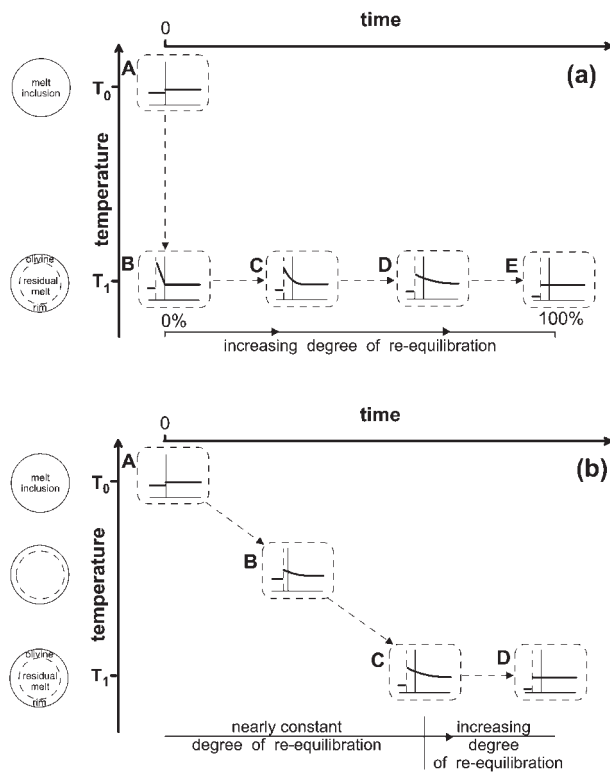


Fig. 1. A schematic representation of compositional and phase changes that occur after trapping in melt inclusions in olivine phenocrysts. The underlying assumption of this model is that the composition of the host olivine does not change after trapping of the inclusion. Zero on the time axis indicates the moment of trapping. T_0 is the temperature of trapping. Temperature difference between T_0 and T_1 is the length of the cooling interval. Schemes to the left of the temperature axis show the phase composition of the melt inclusion at different temperatures. Plots surrounded by thin dashed frames show compositional profiles through the inclusion–host boundary; bold continuous line shows Fe concentrations; continuous vertical line shows the boundary between the initial volume of the melt inclusion and the host; dashed vertical line shows the boundary between the olivine rim on the walls of the inclusion and the residual melt. Plot at point A shows the initial Fe concentrations in the melt inclusion and the host at the moment of trapping. (a) A case of instant cooling, i.e. temperature drops instantaneously from T_0 to T_1 . At point B the melt inclusion consists of the zoned olivine rim and the residual melt. When the inclusion is kept at T_1 (the residence temperature) it gradually re-equilibrates with the host (path B–C–D–E) via diffusion of Fe into the host olivine and Mg in the opposite direction, until re-equilibration is completed at point E. It should be noted that with increasing degree of re-equilibration, the compositional gradient in the rim and surrounding host olivine decreases, accompanied by the decreasing Fe content of the residual melt. A detailed description of the re-equilibration process has been given by Danyushevsky *et al.* (2000). (b) A case of simultaneous cooling and re-equilibration over the same cooling interval as in (a). During cooling at a constant rate (path A–B–C) the width of the olivine rim on the walls of the inclusion increases with falling temperature, but the compositional gradient in the rim is at all times shallower than in the case of instant cooling [point B in (a)]. The degree of re-equilibration remains nearly constant along the path A–B–C, whereas Fe concentration in the residual melt decreases and the length of the diffusion profile in the host olivine increases. If the host phenocryst is kept at T_1 , re-equilibration continues similarly to case (a), until it is completed at point D. (See text for discussion.)

equivalent of the estimate of the parental melt for the Western Group of Tongan high-Ca boninites (Danyushevsky *et al.*, 1995).

The 1 atm olivine liquidus temperature of this composition (i.e. the trapping temperature of the inclusion) is 1421°C (Table 1, No. 2). The composition of the host olivine (i.e. olivine in equilibrium with this melt) is $Fo_{93.09}$. The compositional profile through the olivine rim grown over a cooling interval of 150°C on the walls of an inclusion 50 μm in radius is shown in Fig. 2a. The calculated thickness of the rim is 3.14 μm (see caption to Fig. 2). The composition of the residual melt inside the inclusion is given in Table 1 (No. 2). When the inclusion is kept at 1271°C, re-equilibration with the host begins via diffusion of Fe into the host olivine and Mg in the opposite direction. Diffusion profiles around the inclusion at different degrees of re-equilibration are shown in Fig. 2. It should be noted that with increasing degree of re-equilibration there is a rapid decrease in the compositional gradient next to the inclusion, as well as an increase in the diffusion distance.

From Fig. 2b it can be seen that 20% re-equilibration will be achieved in 12 h, and that nearly complete re-equilibration (i.e. 98%, when differences of Fe contents along the diffusion profile are well within the precision of the microprobe analysis) in 6 months and 9 days (Fig. 2e). Compositions of the residual melt inside the inclusion at 20%, 50%, 80% and 100% re-equilibration are given in Table 1 (Nos 3–6). As the rate of diffusion is dependent on the compositional gradient, 80% re-equilibration occurs within the first 10% of the time required for nearly complete re-equilibration (Fig. 2d and e). The relationship between time and degree of re-equilibration is shown in Fig. 3a for a range of inclusion sizes and cooling intervals.

For a given cooling interval, increasing the size of an inclusion results in (1) a wider olivine rim and thus a shallower initial compositional gradient, and (2) a larger amount of Fe that diffuses from the inclusion for a given degree of re-equilibration, resulting in longer diffusion distances. Both factors result in a longer re-equilibration time. The relationship between re-equilibration time and inclusion size is shown in Fig. 3b for 98% re-equilibration. For a given cooling interval, re-equilibration time is a polynomial function of inclusion radius. As can also be seen from Fig. 3b, increasing the cooling interval results in longer re-equilibration time for a given inclusion size. The relationship between re-equilibration time and cooling interval is shown in Fig. 3c for 98% re-equilibration. For a given inclusion size, re-equilibration time can be approximated as an exponential function of cooling interval. As can be seen in Fig. 3, the effect of inclusion size on re-equilibration time is significantly larger than the effect of cooling interval. The combined effect of these two factors can be described as

Table 1: Compositions of the trapped melts and residual melts inside inclusions for examples described in the Method section

No.	Tonga						Vesuvius	Siqueiros	Belingwe
	1	2	3	4	5	6	7	8	9
Re-equil. (%)	—	0	20	50	80	100	—	—	—
SiO ₂	52.57	55.603	55.997	56.49	56.925	57.184	45.07	48.89	48.05
TiO ₂	0.4	0.506	0.514	0.525	0.534	0.54	0.98	0.76	0.32
Al ₂ O ₃	9.51	12.019	12.221	12.473	12.7	12.838	13.48	15.64	7.22
Fe ₂ O ₃	—	1.236	1.257	1.283	1.306	1.32	—	—	—
FeO	8.61	7.479	6.659	5.625	4.748	4.238	6.99	8.67	10.89
MnO	0.2	0.253	0.257	0.262	0.267	0.27	0.17	0.17	0.11
MgO	19.01	10.771	10.757	10.752	10.7	10.651	6.53	11.99	24.96
CaO	7.62	9.631	9.793	9.994	10.176	10.286	11.21	11.88	6.99
Na ₂ O	1.29	1.63	1.658	1.692	1.723	1.741	1.74	1.84	0.75
K ₂ O	0.59	0.746	0.758	0.774	0.788	0.796	5.01	0.023	0.03
P ₂ O ₅	0.1	0.126	0.129	0.131	0.134	0.135	0.83	0.055	0.07
Fe ²⁺ /Fe ³⁺ init.	8.79	—	—	—	—	—	6.00	9.52	10.4
T (°C)	1422	1271	1271	1272	1272	1271	1203	1286	1508
Fo	93.1	88.3	89.5	91.0	92.3	93.1	87.3	90.0	93.5
Oliv (wt %)	0	20.878	21.896	23.11	24.184	24.822	0	0	0
Oliv (norm %)	32.95	—	—	—	—	—	11.00	22.41	47.15

Fe²⁺/Fe³⁺init, Fe²⁺/Fe³⁺ value of the trapped composition; T (°C), calculated olivine liquidus temperature; Fo, olivine composition in equilibrium with the melt; Oliv (wt %), amount of olivine crystallized on the walls of the inclusion; Oliv (norm %), molar olivine CIPW norm; 1, trapped melt composition (Tongan boninite); 2, residual melt after instant cooling over 150°C; 3–6, residual melt after 20, 50, 80 and 100% of re-equilibration; 7, trapped melt composition [Vesuvius; inclusion VS97-109 from Marianelli *et al.* (1999)]; 8, trapped melt composition [Siqueiros MORB; inclusions S1-OL14-GL2 from Danyushevsky *et al.* (in preparation)]; 9, trapped melt composition [Belingwe komatiite; composition PM/93-5 from Gee *et al.* (in preparation)].

$$t = A \exp(B \times CI) R^2 \quad (1)$$

where t is time, CI is cooling interval (in °C) and R is inclusion radius (in μm). Regression coefficients A and B for four degrees of re-equilibration, the units of time, and the accuracy of the regression are given in Table 2. An example of 98% re-equilibration is shown in Fig. 4a.

It should be noted that equation (1) should not be extrapolated to cooling intervals smaller than $\sim 35^\circ\text{C}$, because at such conditions the relationship between t and CI deviates significantly from the exponential law.

Effect of trapping temperature on re-equilibration time

For the purposes of this study it is more convenient to treat melt composition as an independent factor and

temperature as its function for a given set of other physical characteristics. For a given pressure, the trapping temperature of a melt composition is therefore fixed, and thus cannot be treated independently (see the next section for coupled effects of compositional variations and temperature).

However, the effect of temperature variations alone is relevant when estimating the effect of variable melt H₂O contents on re-equilibration time. The presence of H₂O in the melt causes a fall in its liquidus temperature but has little influence on olivine–melt equilibria (e.g. Ulmer, 1989; Falloon & Danyushevsky, 2000). Thus, for a given amount of olivine crystallization on the walls, the width and composition of the rim will remain nearly the same regardless of melt H₂O content.

Variations in trapping temperature result in differences in the residence temperature for a given cooling interval. As $D_{\text{Fe-Mg}}$ is dependent on temperature, and re-equilibration time is inversely proportional to $D_{\text{Fe-Mg}}$,

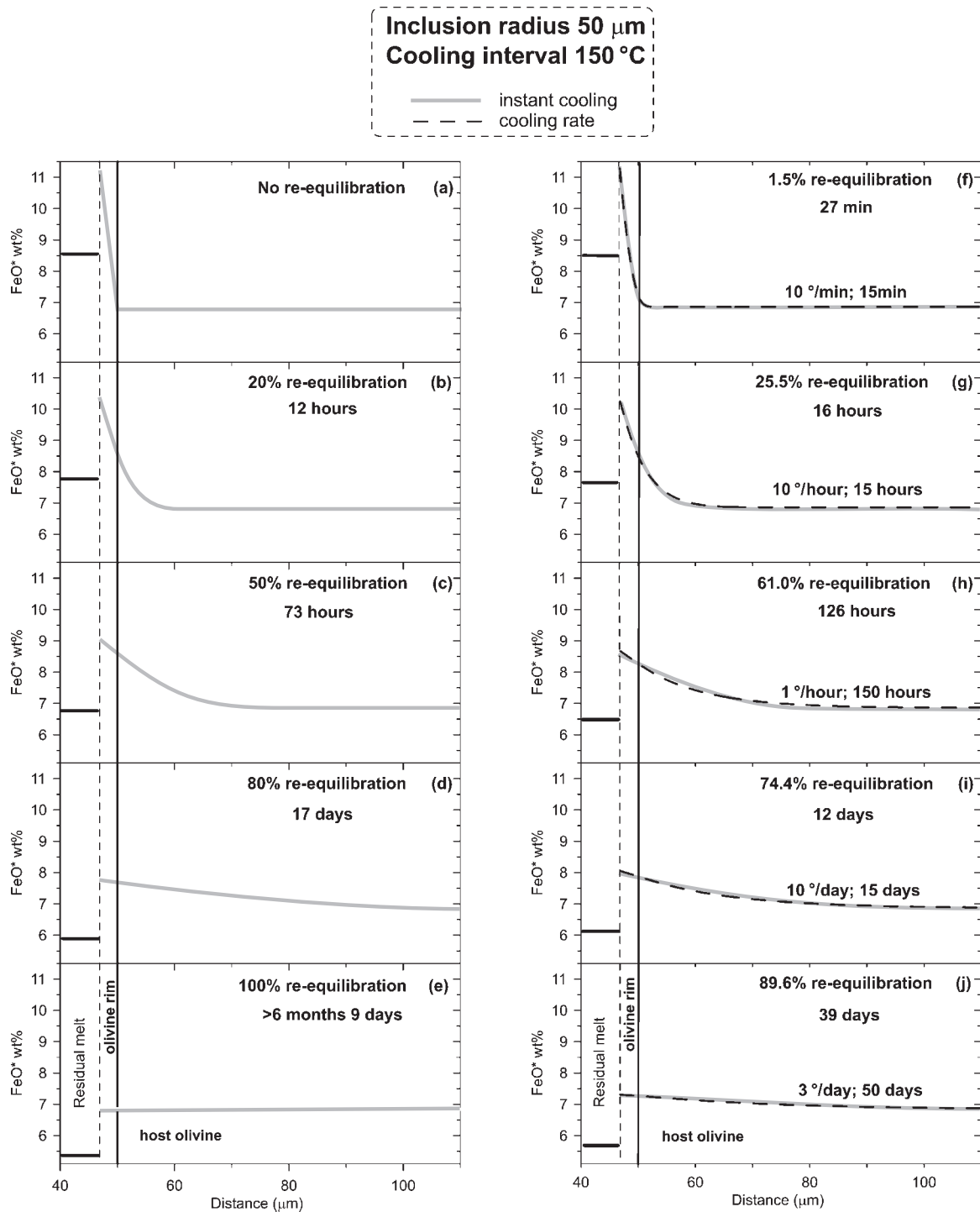


Fig. 2. An example of calculated diffusion profiles through host olivine around a melt inclusion 50 μm in radius cooled over 150 $^{\circ}\text{C}$. Zero on the x-axis corresponds to the centre of the inclusion. Continuous vertical line denotes the boundary between the host olivine and initial volume of the melt inclusion. Dashed vertical line denotes the boundary between the olivine rim on the walls of the inclusion and residual melt inside the inclusion. Olivine rim formed during instant cooling over 150 $^{\circ}\text{C}$ (the initial composition profile) is shown in (a). Width of the olivine rim is estimated from the calculated amount of olivine that crystallized on the walls, assuming olivine density of 3.3 g/cm 3 and the spherical shape of the inclusion. Bold grey line represents profiles formed during re-equilibration at a constant temperature at the lower end of the cooling interval. Re-equilibration times are shown in each plot. Diffusion profiles calculated at five cooling rates are shown as dashed lines in (f)–(j). Cooling rates and the total cooling time are labelled next to each curve. The initial trapped melt composition, trapping temperature, and residual melt compositions at various degrees of re-equilibration are presented in Table 1 (Nos. 2–6). (See text for discussion.)

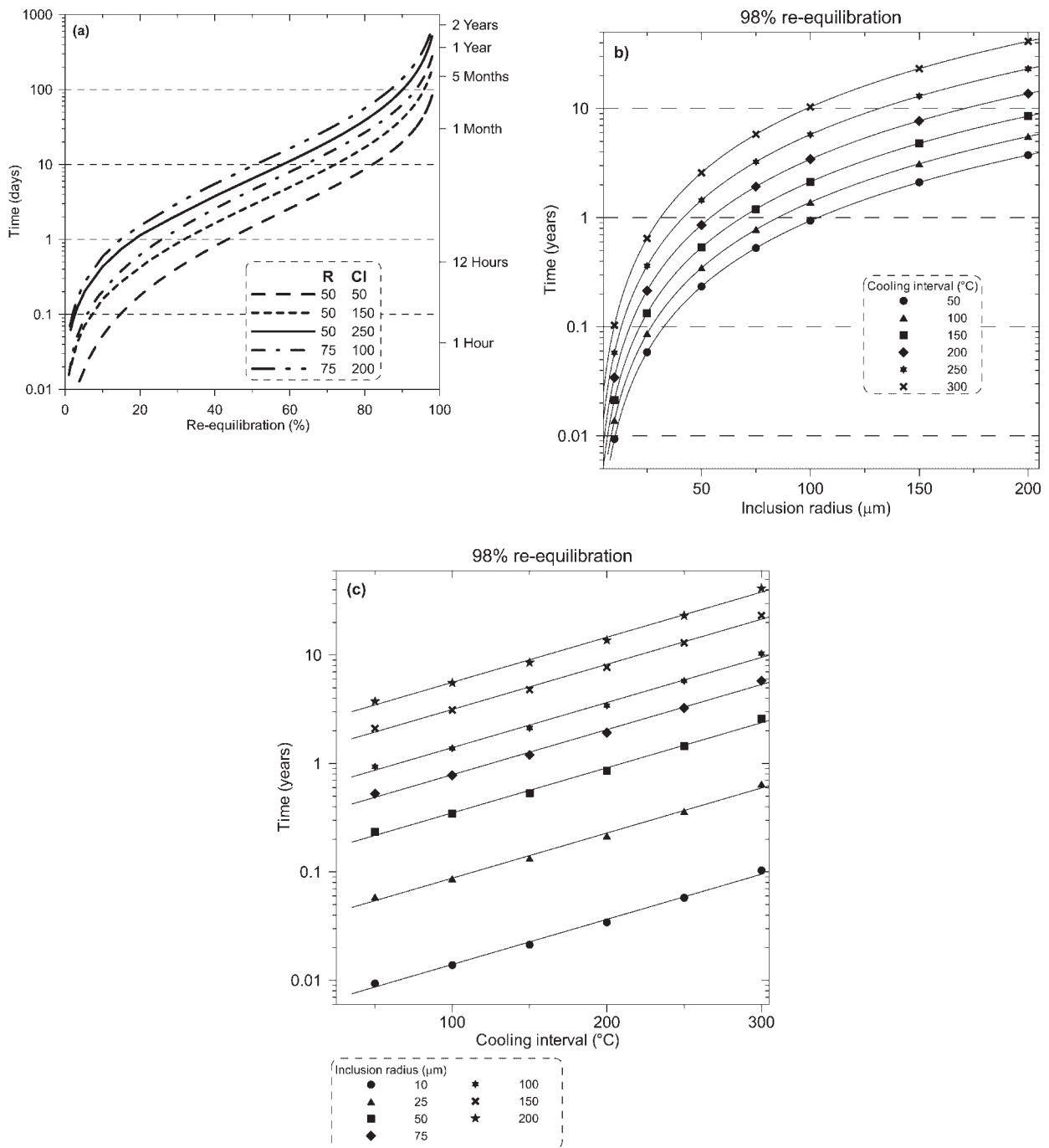


Fig. 3. (a) Relationship between time and degree of re-equilibration for inclusions with the same initial composition (Table 1; No. 1). *R*, inclusion radius in microns; *CI*, cooling interval in °C. In all cases re-equilibration occurs at a constant residence temperature after instant cooling. (b) Relationship between time and inclusion size for 98% re-equilibration. Initial inclusion composition is from Table 1, No. 1. The symbols correspond to different cooling intervals as indicated in the legend. (c) Relationship between time and cooling interval for 98% re-equilibration. Initial inclusion composition is from Table 1, No. 1. The symbols correspond to different inclusion sizes as indicated in the legend.

variations in trapping temperature cause differences in re-equilibration time. According to Chakraborty (1997; see their fig. 5), the relationship between temperature (*T*) and $D_{\text{Fe-Mg}}$ for high-Mg olivines ($\text{Fo} > 86$) is

$$\log(D_{\text{Fe-Mg}}) = -11628/T(\text{K}) - 8.366. \quad (2)$$

The effect of H_2O on olivine liquidus temperature was given by Falloon & Danyushevsky (2000) as

Table 2: Values of regression coefficients for equation (1) for four initial compositions listed in Table 1

Degree of re-equilibration (%)	A	B	Accuracy (%)
<i>Tonga</i>			
98 ^a	5.3390E-05	9.5234E-03	4.8
80 ^b	2.1491E-03	7.9054E-03	4.3
50 ^b	3.6242E-04	8.0178E-03	4.6
20 ^b	3.8620E-05	1.0568E-02	9.5
<i>Vesuvius</i>			
98 ^a	3.3705E-04	1.4942E-02	4.7
80 ^b	8.9658E-03	1.2846E-02	4.6
50 ^b	1.1833E-03	1.2942E-02	4.9
20 ^b	9.8878E-05	1.6206E-02	7.9
<i>Siqueiros</i>			
98 ^a	1.7206E-04	1.2974E-02	3.9
80 ^b	5.8742E-03	1.1186E-02	3.7
50 ^b	8.9388E-04	1.1154E-02	3.9
20 ^b	8.1260E-05	1.4135E-02	7.0
<i>Belingwe</i>			
98 ^a	2.8817E-05	8.8915E-03	2.6
80 ^b	1.3569E-03	7.4776E-03	2.7
50 ^b	2.5678E-04	7.5581E-03	2.3
20 ^b	2.7837E-05	1.0355E-02	6.0

^aCalculated time is in years.

^bCalculated time is in days.

$$\text{liquidus depression } (^{\circ}\text{C}) = 74.403(\text{H}_2\text{O wt } \%)^{0.352}. \quad (3)$$

This latter function is largely independent of temperature and melt composition for mantle-derived magmas. However, as $D_{\text{Fe-Mg}}$ is an exponential function of temperature, the effect of melt H_2O content on re-equilibration time is temperature dependent.

For example, if the H_2O content in the residual melt of the inclusion shown in Fig. 1 was 2 wt %, then the temperature at which re-equilibration occurs would be 1176°C (compared with 1272°C for the anhydrous composition; Table 1). Following (2), the ratio between $D_{\text{Fe-Mg}}$ values at these two temperatures is $D_{\text{Fe-Mg}}(1271^{\circ}\text{C})/D_{\text{Fe-Mg}}(1176^{\circ}\text{C}) = 3.152$. Thus, re-equilibration times will be 3.152 times longer than those calculated for the anhydrous composition (Fig. 1).

Compositional effects on re-equilibration time

Variations in compositions of both the host olivine and the trapped melt cause differences in re-equilibration

time. According to Chakraborty (1997), $D_{\text{Fe-Mg}}$ increases with decreasing Fo content of olivine at $\text{Fo} < 86$. For a given temperature, increase in $D_{\text{Fe-Mg}}$ can be described as

$$D_{\text{Fe-Mg(at Fo}<86)} = D_{\text{Fe-Mg(at Fo=86)}} + 0.03115(100 - \text{Fo}) - 0.456 \quad (4)$$

where $D_{\text{Fe-Mg(at Fo=86)}}$ is the value of $D_{\text{Fe-Mg}}$ from equation (2).

Thus, re-equilibration times of melt inclusions in less forsteritic olivines, all other parameters being equal, will be shorter. This effect appears to be fairly large; the difference in $D_{\text{Fe-Mg}}$ values for Fo_{86} and Fo_{25} is similar to that caused by a temperature rise from 1000°C to 1300°C for a given olivine composition.

Variations in melt composition may result in variations of the Fe–Mg exchange coefficient between olivine and melt (K_d). The effect of K_d on the thickness and composition of the rim for four compositions (Table 1), for a given inclusion radius and cooling interval, is shown in Fig. 5a. The range of K_d values shown (0.25–0.35) is wider than that observed for most mantle-derived magmas at low pressures (e.g. Falloon *et al.*, 1997). Figure 5b shows differences in the thickness and composition of the rim caused by modest variations in inclusion size and cooling interval for a given composition (Tonga, Table 1). It is clear from Fig. 5 that possible variations in the K_d value produce only a minor difference in the thickness and composition of the rim and thus we do not consider the effect of K_d variations further.

On the other hand, differences in melt composition, and in particular in its normative olivine content, will cause significant variations in the thickness of the rim (Table 1, Fig. 5a). This is because the slope of the olivine liquidus (i.e. the amount of olivine crystallized per degree of temperature fall) decreases with decreasing normative olivine content of the melt. A thinner rim formed at a given cooling interval results in smaller changes in the residual melt relative to the originally trapped composition. At the same time, a decrease in melt normative olivine content is accompanied by a fall in melt liquidus temperature, and thus in lower $D_{\text{Fe-Mg}}$ values. The times for nearly complete re-equilibration (98%) of inclusions of four different compositions (Table 1) are shown in Fig. 4. Regression coefficients A and B from equation (1) for four degrees of re-equilibration for each composition, and the accuracy of each regression, are given in Table 2. The four compositions we have chosen mostly cover the range of major element contents in primitive mantle-derived magmas.

Observed differences in re-equilibration time (the longest for a Vesuvius composition and the shortest for a Belingwe komatiite) reflect differences in both re-equilibration temperature and melt composition. The

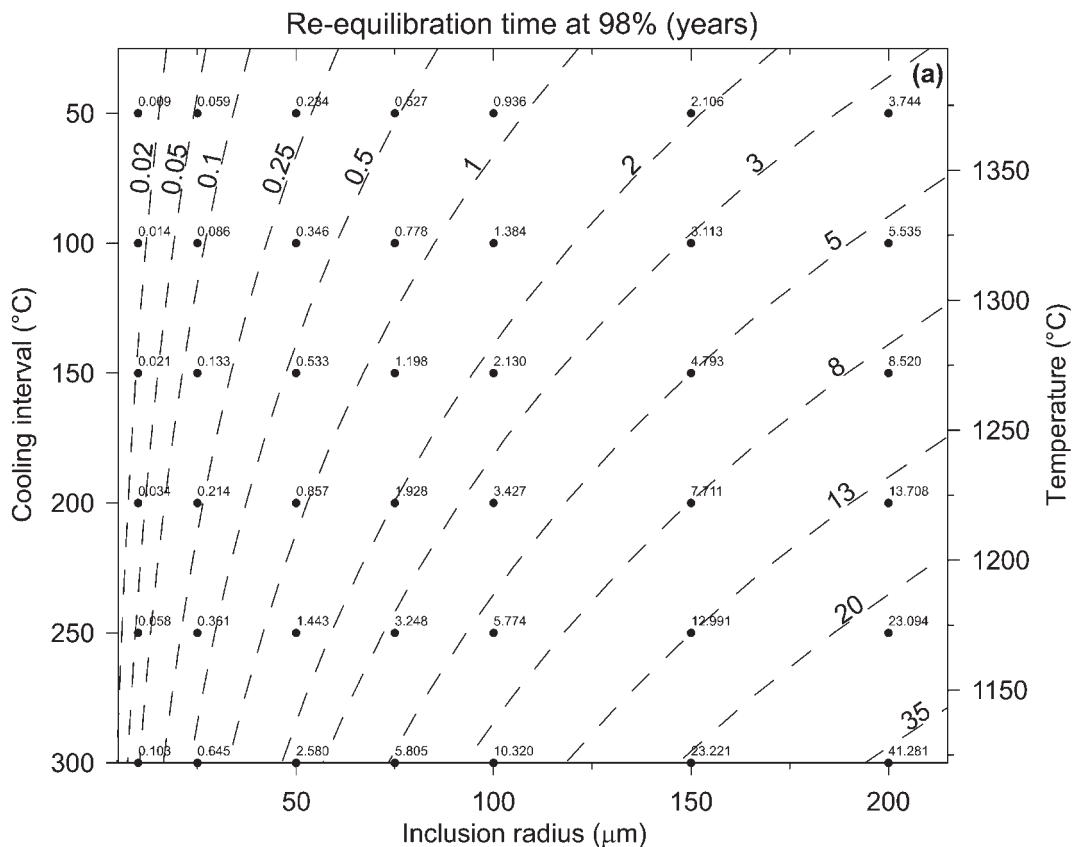


Fig. 4a.

effect of temperature can be removed following the technique described above. Re-equilibration times adjusted to temperatures of the Tonga composition (Fig. 4a) are shown in parentheses in Fig. 4b–d. These adjusted times reflect differences caused by variable melt compositions, whose main effect is to change the amount of olivine crystallization on the walls (i.e. thickness of the rim). For the Vesuvius example, with the thinnest rim, adjusted re-equilibration times are the shortest, whereas for the Belingwe example, where the rim is the thickest, adjusted times are the longest.

Overall, differences in re-equilibration times caused by variations in melt compositions are small (~1.5 times between the longest and the slowest examples), compared with the effects of inclusion size, cooling interval, degree of re-equilibration and trapping temperature.

Effect of variable cooling rates

In the preceding discussion we considered the case of instant cooling, when re-equilibration occurs at a constant residence temperature. In this section we consider the effects of variable cooling rates on re-equilibration times.

In the example described below, the initial trapped melt composition is a Tongan boninite (Table 1, No. 1), the inclusion radius is 50 µm, and the cooling interval is 150°C. Diffusion profiles and compositions of the residual melt inside the inclusion at various degrees of re-equilibration, calculated for the case of instant cooling, are shown in Fig. 1 and Table 1 (Nos 2–6). We performed calculations at five rates; 10°/min, 10°/h, 1°/h, 10°/day and 3°/day. Simultaneous cooling and re-equilibration have been modelled in 15 steps of 10°C each. First, the olivine rim is calculated for the case of instant cooling over 10°C; then re-equilibration is modelled at this temperature for a period of time appropriate for the cooling rate of interest (e.g. for the cooling rate of 10°/min, re-equilibration was modelled for 1 min). Then the next cooling step is calculated.

The results are presented in Fig. 2f–j. The compositional profile for the case of instant cooling (0% re-equilibration) is shown in Fig. 2a. A cooling rate of 10°/min results in 1.5% re-equilibration, and thus this cooling rate corresponds to virtually instant cooling. It should be noted that for inclusions of larger sizes and/or trapped at lower temperatures, the cooling rate corresponding to

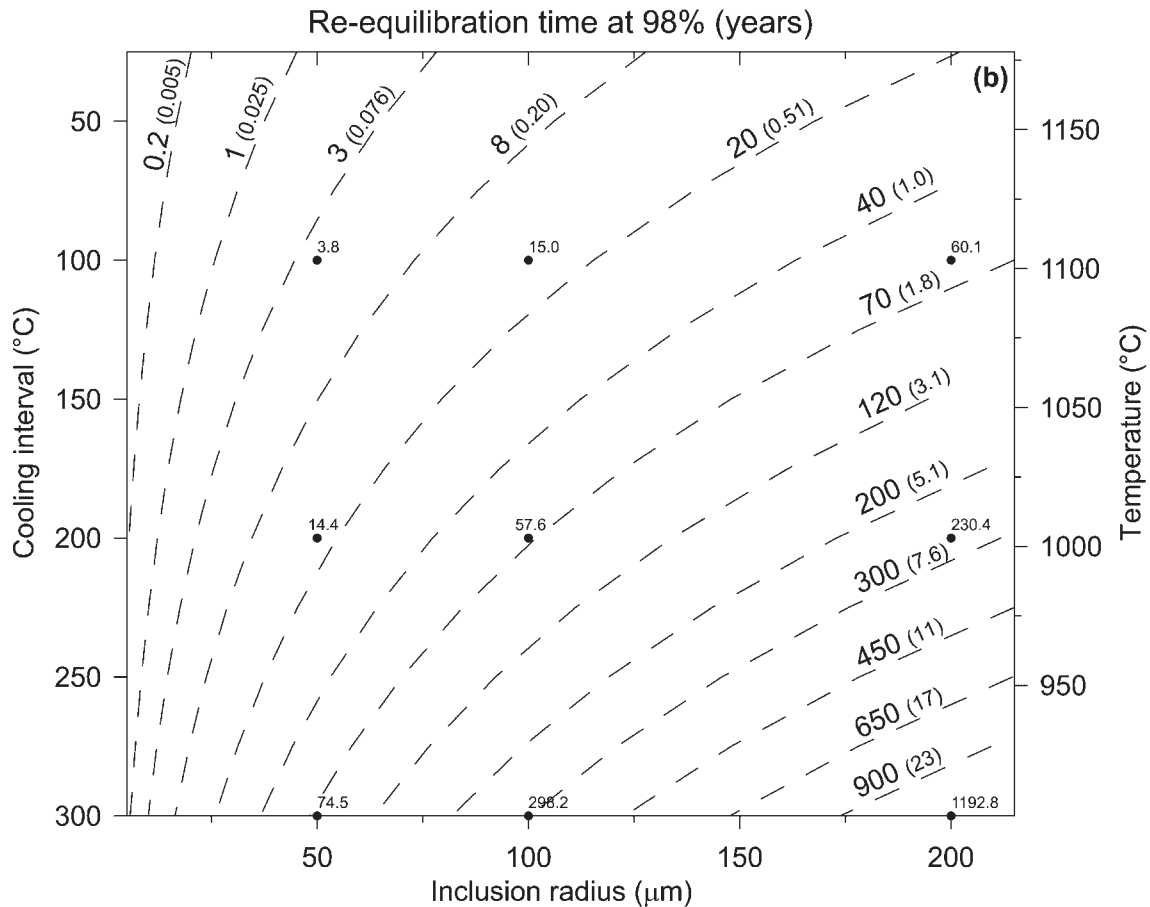


Fig. 4b.

instant cooling will be slower. The cooling rate of $3^\circ/\text{day}$ results in $\sim 89\%$ re-equilibration.

As can be seen in Fig. 2f–j, the shapes of diffusion profiles calculated at variable cooling rates are essentially identical to those of profiles calculated in the case of instant cooling for the same degree of re-equilibration. The differences between them are well within the precision of microprobe analyses. This implies that, in general, diffusion profiles cannot be used to distinguish between these two possible cooling scenarios and thus cannot be used to infer cooling rates. However, at long cooling intervals of $>300^\circ\text{C}$ and large degrees of re-equilibration ($>75\%$) the difference in the shape of diffusion profiles between two cooling scenarios is large enough to be detected by microprobe analyses.

The relationship between times required to achieve a given degree of re-equilibration in cases of instant cooling or an appropriate cooling rate is complex. In general, at higher degrees of re-equilibration and shorter cooling intervals the time is less in the case of instant cooling compared with cooling with an appropriate cooling rate.

However, differences in times between the two cooling scenarios do not appear geologically significant. Apparent cooling rates can thus be reasonably approximated from re-equilibration times calculated for the case of instant cooling [equation (1)] using the total length of the cooling interval.

Deriving residence time from inclusion compositions and diffusion profiles

A time estimate requires data on inclusion size, trapping temperature, cooling interval and degree of re-equilibration.

The cooling interval can be estimated as the difference between temperatures of trapping and diffusion closure. For submarine eruptions and thin subaerial lava flows, effective quenching allows the closure temperature to be approximated by the eruption temperature. The eruption temperature in such cases can be derived from the composition of the groundmass of the sample, or glass

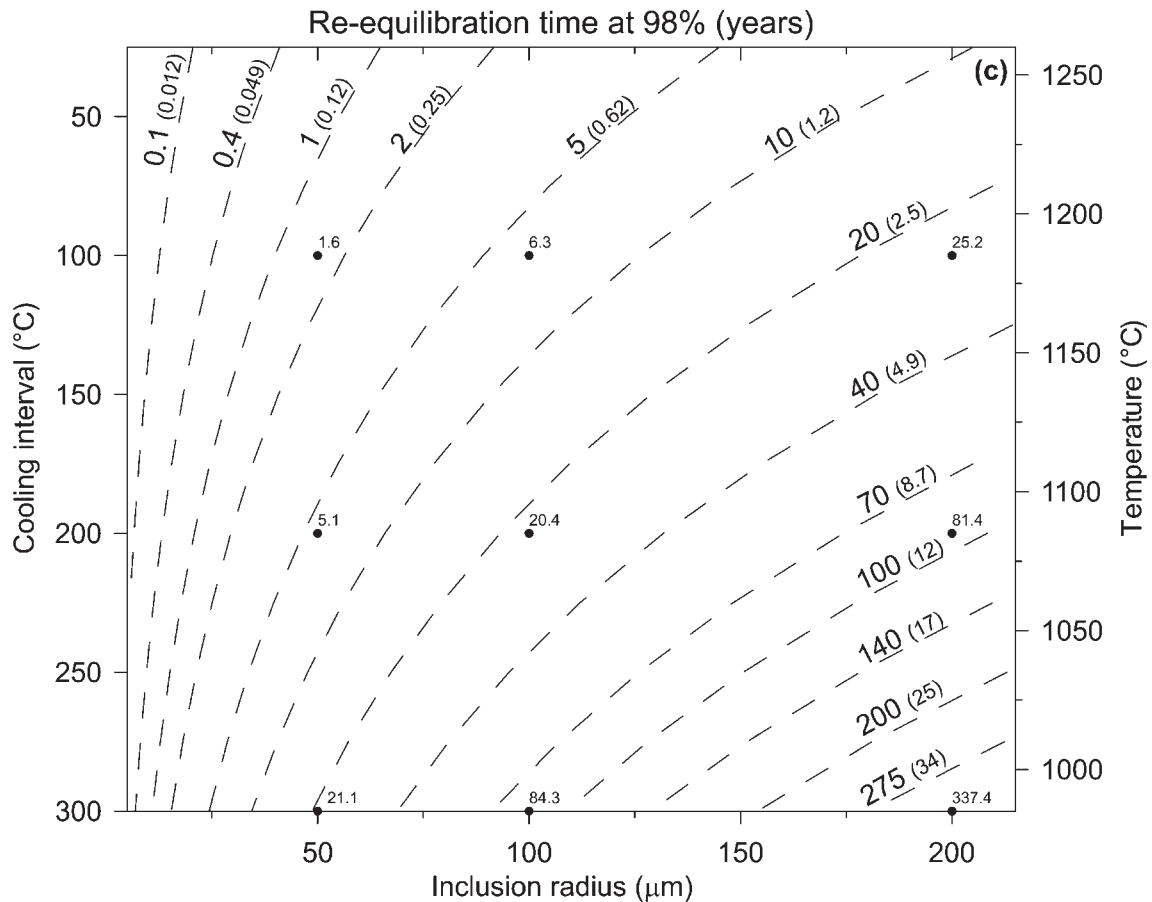


Fig. 4c.

rinds, using mineral–melt equilibrium models (e.g. Ford *et al.*, 1983; Ariskin, 1999). In thick lava flows or lava lakes, however, slow cooling after the eruption results in closure temperatures being lower than the eruption temperature, and in such cases they are more difficult to estimate.

The trapping temperature can either be determined from homogenization experiments [see Danyushevsky *et al.* (2002) for a recent summary of homogenization techniques], or estimated using numerical modelling from the composition of the residual melt inside the inclusion when it is quenched to glass. Numerical modelling of trapping temperature requires an independent estimate of the initial trapped melt FeO* content, which in most cases can be estimated from rock compositions of the volcanic series [see Danyushevsky *et al.* (2000) for a detailed description of the algorithms involved in these calculations].

The degree of re-equilibration can be estimated using two approaches. First, it can be obtained from modelling

of changes to the residual melt composition inside inclusions during re-equilibration. This calculation requires information on the composition of the trapped melt and the length of the cooling interval. The calculation involves choosing a degree of re-equilibration that results in the FeO* content of the residual melt matching the value measured in the inclusion. Re-equilibration time can then be interpolated from values calculated for 20%, 50%, and 80% re-equilibration using equation (1) for the appropriate composition. As can be seen in Fig. 3a, $\log(t)$ is a nearly linear function of the degree of re-equilibration between ~15% and ~90%, making interpolation straightforward. In cases when trapping temperature differs from that of the four compositions described above, a temperature correction will have to be introduced as described above.

The second approach is more complex and time consuming, but it provides a more precise time estimate. It involves first analysing the diffusion profile in the host olivine around the inclusion, and then matching it to a

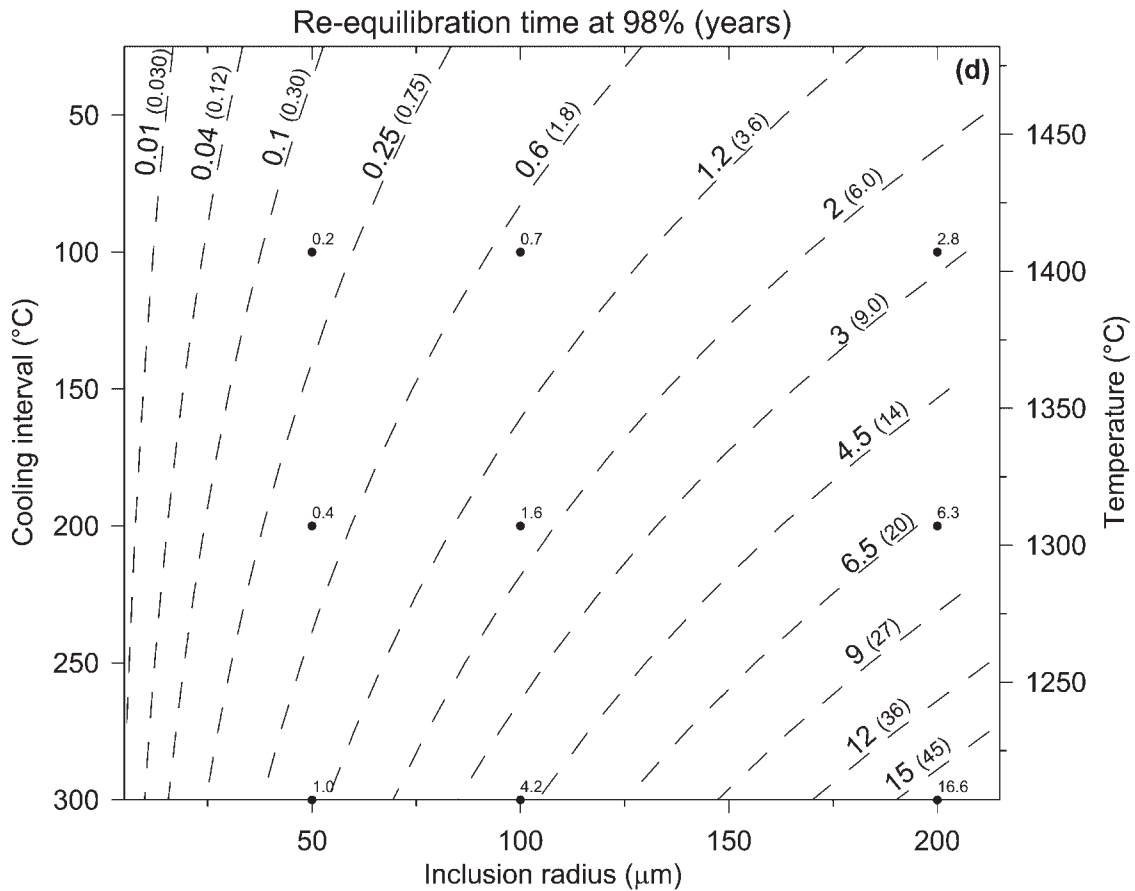


Fig. 4d. Relationship between time, inclusion size and cooling interval for 98% re-equilibration. ●, combinations of cooling interval and inclusion sizes for which calculations were performed; labels next to dots show time in years. Dashed lines show isochrones calculated from equation (1) using regression coefficients from Table 2; labels indicate time in years; values in parentheses next to labels in (b)–(d) show re-equilibration time if diffusion occurred at the same temperature as in (a). (See text for discussion.) (a) Initial inclusion composition is a primitive Tongan boninite (Table 1, No. 1); (b) initial inclusion composition is a primitive melt from Vesuvius (Table 1, No. 7); (c) initial inclusion composition is a primitive MORB from Siqueiros transform fault (Table 1, No. 8); (d) initial inclusion composition is a Belingwe komatiite (Table 1, No. 9).

profile calculated during modelling of the diffusion process. The input parameters for calculation are the initial trapped composition of the inclusion, inclusion size, cooling interval and cooling rate. Computer programs that perform these calculations are available from the first author.

When no diffusion profile is observed in the host olivine around the inclusion, this indicates either a nearly complete re-equilibration or lack of re-equilibration. These two cases can be distinguished by the FeO* content of the residual melt, which should be unrealistically low in the former case. An apparent lack of re-equilibration does not necessarily imply very fast cooling and immediate quenching; it can also occur in cases of very small cooling intervals, when the difference between the temperature of trapping and quenching is $<25^{\circ}\text{C}$.

EXAMPLES OF MELT INCLUSIONS FROM VARIOUS MAGMA TYPES

Mid-ocean ridge basalt from the Siqueiros transform fault, East Pacific Rise

Sample ALV-2384-3 is a basalt with $\sim 10\%$ of unzoned olivine phenocrysts ranging in composition from Fo_{89-3} to Fo_{91-2} (Perfit *et al.*, 1996; Danyushevsky *et al.*, in preparation). Olivine phenocrysts contain naturally quenched glassy melt inclusions. Figure 6a shows two compositional profiles analysed at two opposite sides of a melt inclusion $\sim 50\ \mu\text{m}$ in radius in olivine phenocryst S1/OL63 ($\text{Fo}_{90.7}$). Along both profiles, there is a clear increase in FeO content and decrease in MgO content within $\sim 10\ \mu\text{m}$ from the inclusions. The symmetrical shape of the profiles indicates that they do not represent a compositional zoning of the phenocrysts but are frozen

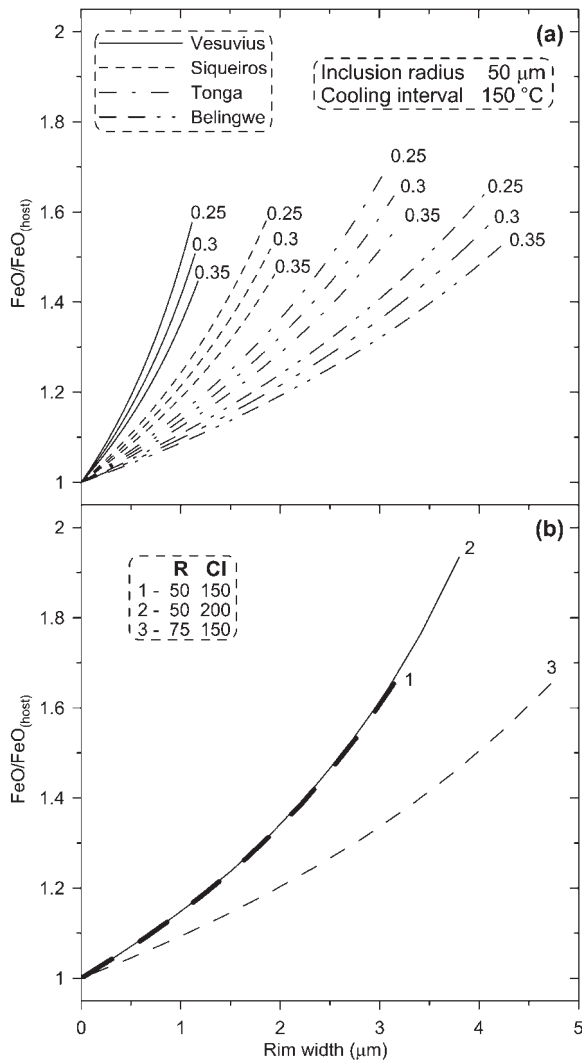


Fig. 5. Effect of the trapped melt composition on the width and composition of the olivine rim on the walls of the inclusion. (a) Calculated compositions of olivine rim grown over cooling interval of $150^\circ C$ on the walls of an inclusion $50 \mu m$ in radius. Zero value on the x-axis corresponds to the boundary between inclusion and its host; labels next to each curve show values of olivine-melt $K_d^{(Fe-Mg)}$. Continuous lines, melt inclusion in olivine $FO_{87.3}$ from 1944 eruption of Vesuvius (Marianelli *et al.*, 1999; Table 1, No. 7); dashed lines, melt inclusion in olivine $FO_{90.0}$ from MORB from Siqueiros Fracture Zone (Danyushevsky *et al.*, in preparation; Table 1, No. 8); dash-dotted line, parental melt composition for the western group of Tongan boninites (Table 1, No. 1); double dash-double dotted line, parental melt composition for Belingwe komatiites (Gee *et al.*, in preparation; Table 1, No. 9). (b) Dependence of the composition of olivine rim on cooling interval and inclusion size. R, inclusion radius in microns; CI, cooling interval in $^\circ C$. The rim was calculated using parental melt for the western group of Tongan boninites as the initial inclusion composition [dash-dotted curves in (a)] following the olivine-melt equilibrium model of Ford *et al.* (1983). Curve 1 is from Fig. 2a. The figure demonstrates that variations in melt composition (mainly the amount of normative olivine) have a significant effect on the width of the olivine rim (a) compared with the effect of cooling interval and inclusion size (b). On the other hand, difference in olivine-melt $K_d^{(Fe-Mg)}$ values have an insignificant effect on the rim width and composition. (See text for further discussion.)

diffusion profiles resulting from re-equilibration of the melt inclusion with its host. The composition of the residual melt inside the inclusion (represented by quenched glass) is presented in Table 3, No. 1. Diffusion profiles have been analysed around seven melt inclusions in different grains, and all of them have similar shapes. The complete dataset is available from the first author. It should be noted that the low MgO and FeO contents of the glass next to the olivine rim (Fig. 6a) are a result of quench modifications (fast disequilibrium growth of olivine on the walls of the inclusion during quenching, which depletes the adjacent melt in MgO and FeO). Such quenching 'troughs' are normally observed in both naturally and experimentally quenched melt inclusions (Fig. 6) and extend up to $5-6 \mu m$ from the walls.

The composition of the pillow-rim glass of the sample can be used to estimate the eruption temperature ($1231^\circ C$, Table 3, No. 2) which represents the low-temperature end of the cooling interval. The lower MgO content of the quenched glass inside the inclusion compared with the pillow-rim glass, yielding lower calculated olivine liquidus temperature ($1215^\circ C$, Table 3, No. 1), is a result of olivine crystallization during eruption, which is more pronounced in the inclusions as a result of their high surface area of the boundary between liquid and solid. This olivine forms a thin ($\sim 0.2 \mu m$) rim on the walls of the inclusion. The composition of the residual melt inside the inclusion at the moment of eruption can be calculated by modelling the reverse of olivine fractionation [Table 3, No. 3; see appendix in Danyushevsky *et al.* (2000) for the calculation technique; all calculations in this section are performed with a melt Fe^{2+}/Fe^{3+} value of 9.52]. This residual melt has lower FeO^* content than the pillow-rim glass, a result of re-equilibration with the host as evidenced by the diffusion profiles (Fig. 6a).

The pillow-rim glass composition is in equilibrium with olivine $FO_{88.6}$. This indicates that phenocryst S1/OL63 crystallized from a more primitive melt than is represented by the pillow-rim glass. As olivine and spinel are the only liquidus phases of the pillow-rim glass composition (Perfit *et al.*, 1996; Danyushevsky *et al.*, in preparation), it is straightforward to calculate the crystallization path of the magma by modelling the reverse of olivine fractionation. The FeO^* content of the melt in equilibrium with $FO_{90.7}$ (the composition of phenocryst S1/OL63) is ~ 8.2 wt %. This estimated value of the melt FeO^* content at the moment of trapping allows calculation of the trapped melt composition and the temperature of trapping (Table 3, No. 4; see the previous section for calculation details). The trapping temperature represents the high-temperature end of the cooling interval of the phenocryst, which was $60^\circ C$.

The calculated compositions of the residual melt inside the inclusion at 0% and 100% re-equilibration after

Table 3: Compositions of melt inclusions described in the section 'Examples of melt inclusions from various magma types'

	Siqueiros MORB							Hunter arc tholeiites			Bellingwe komatiites			Tongan boninites					
	1	2	3	4	5	6	7	8	9	10	11	12	13	14	15	16	17	18	19
SiO ₂	49.33	49.19	49.20	48.55	49.04	49.48	52.73	51.95	54.01	49.44	53.91	53.83	59.00	56.13	58.51	50.81	56.72	59.11	58.74
TiO ₂	0.89	0.99	0.88	0.82	0.87	0.89	0.37	0.44	0.57	0.41	0.56	0.36	0.29	0.49	0.28	0.16	0.26	0.29	0.28
Al ₂ O ₃	17.76	17.15	17.50	16.31	17.35	17.79	11.73	12.41	12.00	8.66	11.92	9.63	12.64	13.57	12.29	7.22	11.50	12.56	12.39
FeO*	7.56	8.06	7.60	8.20	8.08	6.78	7.49	7.83	5.76	11.64	5.95	9.71	5.44	10.36	5.54	9.27	9.34	4.31	4.98
MnO	0.15	0.17	0.15	0.14	0.15	0.15	0.15	0.17	0.09	0.10	0.09	0.19	0.18	0.20	0.17	0.15	0.17	0.17	0.17
MgO	9.15	9.60	9.71	12.05	9.68	9.71	16.56	14.49	14.21	20.01	14.29	16.30	7.16	6.03	8.34	23.50	8.07	8.37	8.42
CaO	12.79	12.39	12.61	11.75	12.50	12.81	7.87	10.12	11.86	8.61	11.78	8.50	14.16	11.16	13.77	8.15	12.90	14.07	13.88
Na ₂ O	2.23	2.33	2.20	2.05	2.18	2.24	2.30	2.19	1.27	0.92	1.27	1.27	0.95	1.82	0.92	0.54	0.87	0.94	0.93
K ₂ O	0.03	0.03	0.03	0.03	0.03	0.03	0.52	0.29	0.06	0.05	0.07	0.16	0.16	0.21	0.16	0.09	0.15	0.16	0.16
P ₂ O ₅	0.04	0.03	0.04	0.03	0.03	0.03	0.06	0.06	0.05	0.04	0.06	0.04	—	—	—	—	—	—	—
Cr ₂ O ₃	0.08	0.06	0.08	0.07	0.07	0.08	0.21	0.06	0.11	0.13	0.11	—	0.02	0.04	0.02	0.10	0.03	0.02	0.05
Total ^a	100.66	99.77	—	—	—	—	98.55	94.57	98.86	—	—	99.76	96.36	96.62	—	—	—	—	—
T (°C) ^b	1215	1231	1231	1290	1230	1230	—	1351 ^c	1324 ^c	1430	1325 ^c	—	—	1060 ^d	1060 ^d	1382 ^b	1060 ^d	1060 ^d	1060 ^d
Fo(host)	90.66	—	90.66	90.66	90.66	90.66	—	93.17	91.34	91.34	91.34	—	94.00	—	94.00	94.00	94.00	94.00	94.00
Fo(calc) ^b	—	88.6	89.3	90.7	88.7	90.7	—	92.4	94.6	91.3	94.5	—	—	76.3	91.4	94.0	83.50	94.00	91.90
Oliv (norm %)	—	—	—	—	—	—	24.97	25.08	—	—	—	—	—	—	—	—	—	—	—

T (°C), calculated olivine liquidus temperature; Fo(host), composition of the host olivine; Fo(calc), calculated composition of olivine in equilibrium with the melt; Oliv (norm %), molar olivine CIPW norm; 1, glass in inclusion S1/OL63 (from Danyushevsky *et al.*, in preparation); 2, pillow-rim glass of sample ALV-2384-3 (from Danyushevsky *et al.*, in preparation); 3, calculated residual melt inside inclusion S1/OL63 at the moment of eruption; 4, calculated trapped melt composition for inclusion S1/OL63; 5, calculated residual melt inside inclusion S1/OL63 at the moment of eruption for 0% re-equilibration; 6, calculated residual melt inside inclusion S1/OL63 at the moments of eruption for 100% re-equilibration; 7, sample D2-1; 8, residual melt in inclusion B1/OL9 that was experimentally reheated to 1250°C and quenched; 9, residual melt in inclusion MGZ8/OL3-2 that was experimentally reheated to 1300°C and quenched; 10, calculated trapped melt composition for inclusion MGZ8/OL3-2 (from Gee *et al.*, in preparation); 11, calculated residual melt composition for inclusion MGZ8/OL3-2 re-equilibrated to 92% at 1080°C and then reheated to 1300°C; 12, sample 5-25 (from Falloon *et al.*, 1989); 13, glass in inclusion 5-25/OL3; 14, pillow-rim glass of sample 5-25 (from Sobolev & Danyushevsky, 1994); 15, calculated residual melt inside inclusion 5-25/OL3 at the moment of eruption; 16, calculated trapped melt composition for inclusion 5-25/OL3; 17, calculated residual melt inside inclusion 5-25/OL3 at the moment of eruption for 0% re-equilibration; 18, calculated residual melt inside inclusion 5-25/OL3 at the moments of eruption for 100% re-equilibration; 19, calculated residual melt inside inclusion 5-25/OL3 at the moments of eruption for 86% re-equilibration.

^aAll compositions recalculated to 100%; totals are of original analyses.

^bTemperatures and olivine compositions are calculated for 1 atm using olivine-melt equilibrium model of Ford *et al.* (1983) and melt Fe²⁺/Fe³⁺ values of 9.52, 7, 10.4 and 9 for Siqueiros, Hunter, Bellingwe and Tongan samples, respectively.

^cCalculated temperatures are higher than experimental temperatures as a result of the presence of H₂O in the melt.

^dTemperatures calculated taking into account melt H₂O contents, as described in the text.

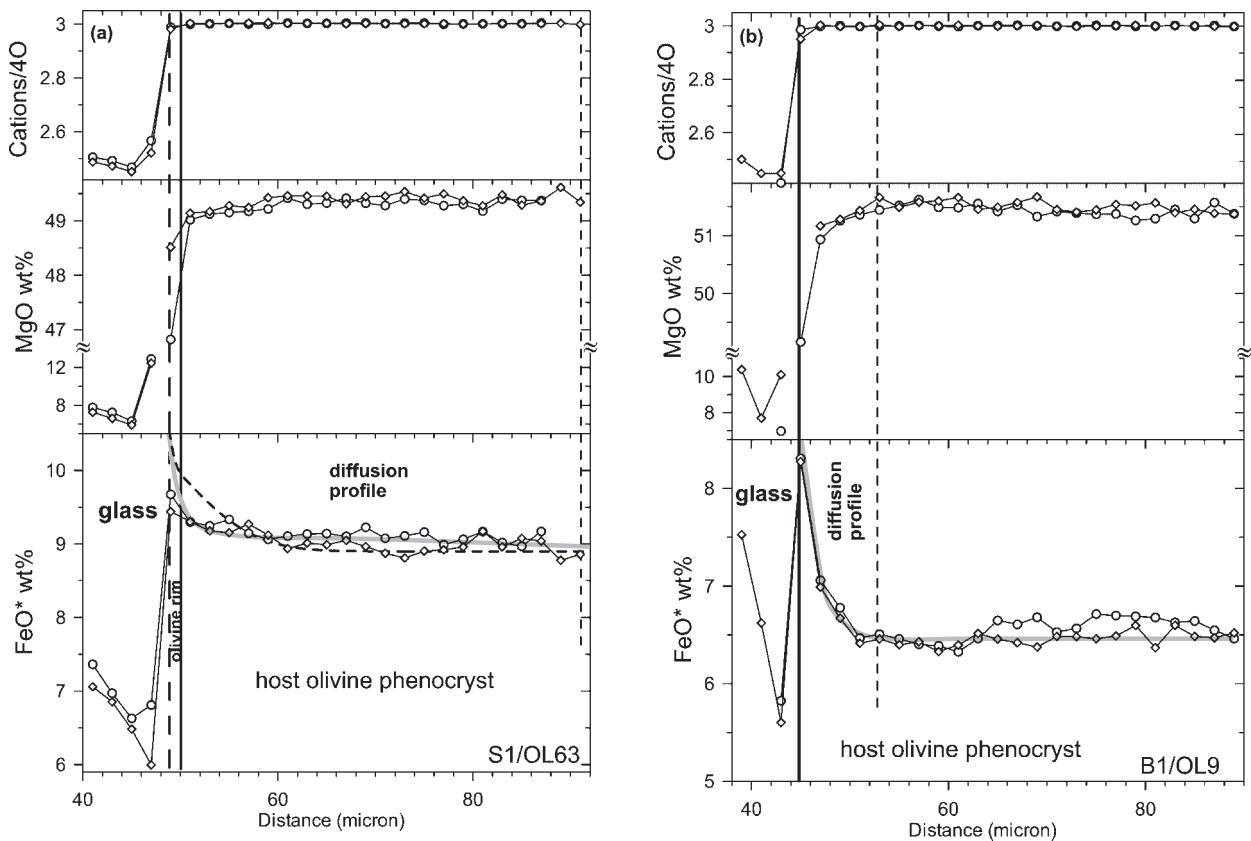


Fig. 6a, b.

cooling over 60°C are shown in Table 3 (Nos 5 and 6). The degree of re-equilibration of inclusion S1/OL63 is the amount of FeO^* 'lost' by the residual melt relative to the amount that is 'lost' in the case of complete re-equilibration, i.e. $100 \times (8.08 - 7.60) / (8.08 - 6.78)$, which is $\sim 35\%$.

The diffusion profile around the inclusion, calculated for cases of (1) instant cooling over 60°C and residence at 1230°C for 1.8 days and (2) cooling over 60°C at a rate of $22^{\circ}/\text{day}$ (both resulting in 35% re-equilibration), is shown in Fig. 6a by a black dashed line. It is clear that this line does not fit the observed profile. The observed profile can be successfully reproduced during the following cooling history: (1) instant cooling from 1290°C to 1260°C and residence at this temperature for ~ 22.5 days, resulting in 70% re-equilibration and $\sim 0.6 \mu\text{m}$ rim thickness (the same can be achieved by cooling over 30°C at a rate of $1^{\circ}/\text{day}$); followed by (2) instant cooling from 1260°C to 1230°C and residence at this temperature for ~ 3 h, resulting in 10% re-equilibration and $\sim 0.4 \mu\text{m}$ rim (the same can be achieved by cooling over 30°C at a rate of $10^{\circ}/\text{h}$). These two steps result in total re-equilibration of 35%. After that, olivine growth during the eruption (equivalent to instant

cooling over 15°C) forms an extra rim $\sim 0.2 \mu\text{m}$ thick, as described above.

The total residence time of this grain at temperatures below its crystallization temperature was ~ 23 days.

Arc tholeiites from the Hunter Ridge, SW Pacific

Arc tholeiites have been dredged from the southern end of the Hunter Ridge, a submarine island arc that defines the southeastern margin of the North Fiji backarc basin between the islands of Fiji and Hunter. The complete set of samples recovered from the area was described by Sigurdsson *et al.* (1993). Sample D2-1 (Table 3, No. 7) is a highly vesicular picrite with $\sim 15\%$ of olivine phenocrysts with core compositions ranging from $\text{Fo}_{93.5}$ to Fo_{83} .

Residual melt in the inclusions from this sample is recrystallized to a coarse aggregate, and thus melt inclusions have been experimentally reheated to 1250°C and quenched after 30 s. The composition of the quenched residual melt in an inclusion of radius $45 \mu\text{m}$ in phenocryst B1/OL9 ($\text{Fo}_{93.2}$) is shown in Table 2 (No. 8). Although experimental temperature has been

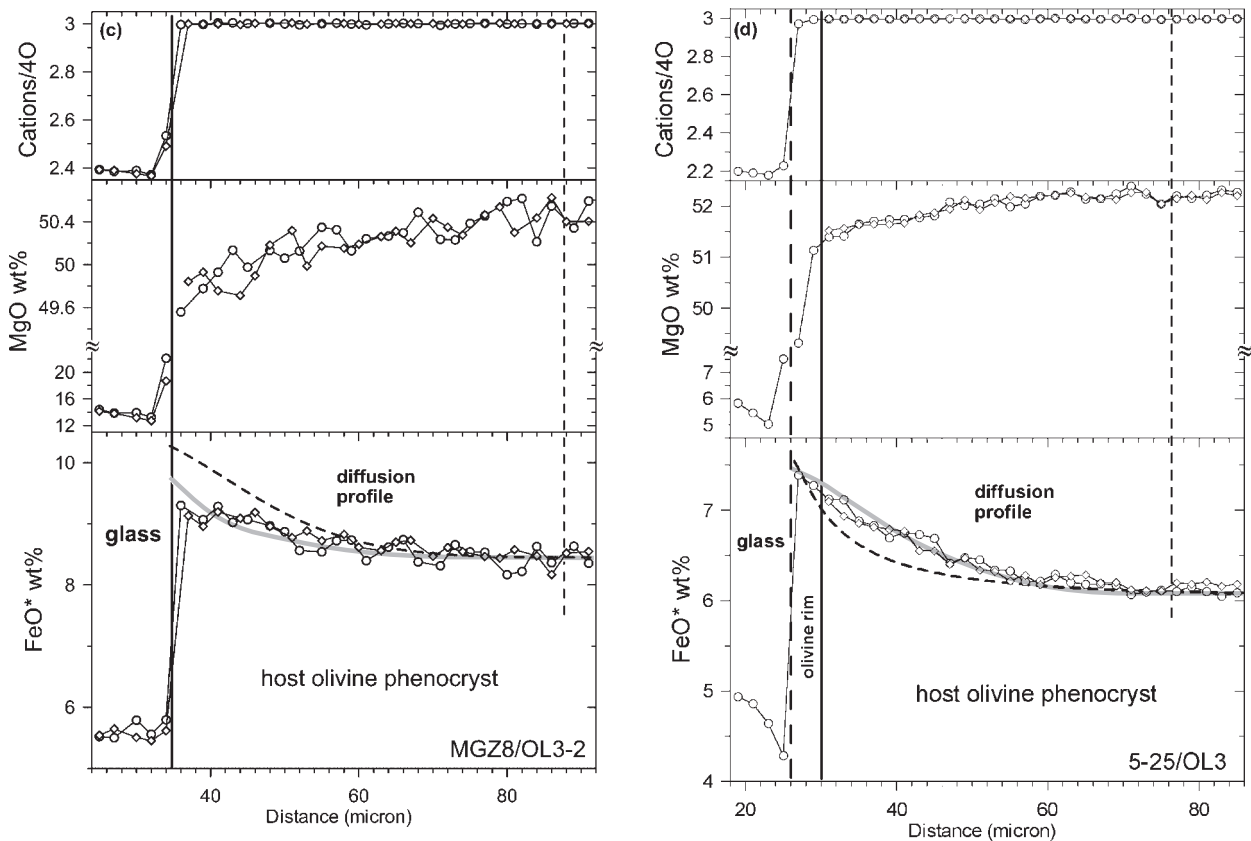


Fig. 6c, d. Compositional profiles through host olivine adjacent to melt inclusions. Profiles have been measured on two sides of inclusions. Electron microprobe analyses were performed at 15 kV, 50 nA, using the minimum beam size ($\sim 2 \mu\text{m}$) and $2 \mu\text{m}$ step. Counting times were 30 and 15 s for Fe (for peak and background, respectively) and 20 and 10 s for Mg and Si. Position of the glass–olivine boundary along the profiles is determined using stoichiometry (Danyushevsky *et al.*, 2000). Analyses at the boundary are affected by the analytical overlap between glass and olivine, and thus FeO^* contents in olivine next to glass are higher than the analysed values. Continuous vertical line defines the inclusion–host boundary. For unheated inclusions, bold dashed vertical line defines the boundary between the residual melt and the olivine rim on the walls of the inclusions. Width of the olivine rim is estimated from the calculated amount of olivine that crystallized on the walls after trapping, assuming olivine density of 3.3 g/cm^3 , melt density of 2.65 g/cm^3 , and spherical shapes of the inclusions. Thin dashed vertical line indicates the width of the diffusion profile. The grey line in FeO^* plots in Fig. 6a, c, and d shows our modelling as described in the text. (a) Naturally quenched melt inclusion S1/OL63 (radius $50 \mu\text{m}$) from sample ALV-2384-3, Siqueiros MORB; dashed black curve shows the diffusion profile calculated for the case of instant cooling over 60°C followed by residence at 1230°C for 1–8 days, resulting in 35% re-equilibration. (b) Experimentally reheated melt inclusion B1/OL9 (radius $45 \mu\text{m}$) from sample D2-1, Hunter Ridge arc tholeiites. (c) Experimentally reheated melt inclusion OL3-2 (radius $35 \mu\text{m}$) from sample MGZ8, Belingwe komatiites; dashed black curve shows the diffusion profile calculated for the case of instant cooling over 350°C followed by residence at 1080°C for 202 days, resulting in 92% re-equilibration. (d) Naturally quenched melt inclusion OL3 (radius $30 \mu\text{m}$) from sample 5-25, Tongan high-Ca boninites; dashed black curve shows the diffusion profile calculated for the case of cooling at a rate of $4^\circ/\text{day}$.

arbitrarily chosen and is probably lower than the trapping temperature, such reheating effectively removes the olivine rim from the walls of the inclusion. Figure 6b presents compositional profiles through the host olivine around this inclusion. Diffusion profiles have been analysed around nine experimentally reheated melt inclusions in high- F_0 phenocrysts ($F_{0.93-0.90}$), and all of them have similar shapes. The complete dataset is available from the first author.

The major element composition of the residual melt in inclusion B1/OL9 and its normative olivine content are close to those of the Tongan boninites (Table 1), and

thus calculations of the re-equilibration times for the latter can be used for this sample. A steep and narrow shape of the diffusion profile (Fig. 6b) indicates small degrees of re-equilibration, between 10 and 20% (compare Fig. 2). Also, the significant increase of FeO content observed along the profile next to the inclusion ($\sim 2 \text{ wt} \%$, Fig. 6b) implies a substantial cooling interval, of the order of $150\text{--}200^\circ\text{C}$ (compare Fig. 2), because this determines the initial gradient in the rim. For the case of Tongan boninites described above, the residence time of a $45 \mu\text{m}$, 20% re-equilibrated inclusion cooled over 200°C is 15.5 h [equation (1), Table 2].

The trapping temperature of inclusion B1/OL9 was lower than that in the above example of the anhydrous analogue of Tongan boninites. This is because (1) primitive melts of Hunter tholeiites had ~ 2.5 wt % H_2O (Sobolev & Chaussidon, 1996), and (2) olivines of a given composition crystallized from a lower MgO melt, compared with Tongan boninites, as a result of the lower FeO contents of the Hunter suite (by ~ 1 wt %, Tables 1 and 3). The effect of 2.5 wt % H_2O on olivine liquidus is $\sim 100^\circ\text{C}$ [equation (3)], and the effect of 1 wt % FeO is $\sim 30^\circ\text{C}$. Thus assuming that the trapping temperature of inclusion B1/OL9 was 150°C lower yields a maximum estimate of residence time of ~ 4.8 days (see above for the effect of trapping temperature on re-equilibration time).

Belingwe komatiites

Fresh, olivine-phyric komatiites have been recovered from and near the SASKMAR 1 drill hole in Belingwe, Zimbabwe (Nisbet *et al.*, 1987; Gee *et al.*, in preparation). Olivine phenocrysts have large unzoned cores surrounded by narrow normally zoned rims (Renner *et al.*, 1994). Core compositions range from $\text{Fo}_{93.5}$ to Fo_{90} .

Residual melt in the inclusions from this sample is recrystallized, and thus melt inclusions have been experimentally reheated to 1300°C and quenched after 30 s [see Gee *et al.* (in preparation) for a detailed description of experimental procedures]. The composition of the quenched residual melt in an inclusion $35\ \mu\text{m}$ in radius in phenocryst MGZ8/OL3-2 ($\text{Fo}_{91.3}$) is shown in Table 3 (No. 9). Figure 6c presents compositional profiles through the host olivine around this inclusion. Diffusion profiles have been analysed around eight experimentally reheated melt inclusions in olivines (Fo_{92-91}), and all of them have similar shapes. The complete dataset is available from the first author.

The calculated trapped composition of this inclusion is shown in Table 3 [No. 10, calculation details have been given by Gee *et al.* (in preparation)]. The observed diffusion profile around the inclusion can be reproduced at a cooling rate of $4.5^\circ\text{C}/\text{day}$ over a cooling interval of 350°C (from 1430 to 1080°C), amounting to a total cooling time of ~ 78 days (Fig. 6c). These conditions result in $\sim 92\%$ re-equilibration. The calculated residual melt composition (Table 3, No. 11, modelled as re-equilibration to 92% at 1080°C and then reheating to 1300°C) matches closely the measured composition. The diffusion profile calculated for the case of instant cooling over 350°C and subsequent residence at 1080°C for 202 days to achieve 92% re-equilibration does not fit the analysed profile (Fig. 6c), and thus the cooling history can be constrained in this case. Cooling occurred at a nearly constant rate over the entire cooling interval, probably within a komatiite lava flow after the eruption.

Tongan high-Ca boninites

A suite of high-Ca boninites dredged from the fore-arc region at the northern termination of the Tonga arc has been described in detail by Falloon *et al.* (1989), Falloon & Crawford (1991), Sobolev & Danyushevsky (1994) and Danyushevsky *et al.* (1995). Danyushevsky *et al.* (2000) provided a detailed description of 'Fe-loss' in melt inclusions in olivine phenocrysts from the Western Group samples of the suite and concluded that they recorded a degree of re-equilibration of $\sim 20\%$. Danyushevsky *et al.* (2000) calculated that this degree of re-equilibration was achieved during residence at a temperature below trapping for <17 days.

Sample 5-25 from the Eastern Group of the suite (Table 3, No. 12) has been described in detail by Falloon *et al.* (1989) and Danyushevsky *et al.* (1995). Compositions of olivine phenocryst cores from this sample display a bimodal distribution with $\sim 70\%$ of compositions between $\text{Fo}_{92.5}$ and Fo_{94} . Phenocrysts from this group (up to 3 mm in size) have unzoned cores surrounded by narrow normally zoned rims, and contain naturally quenched glassy melt inclusions. Major element composition of the residual glass in inclusion 5-25/OL3 ($30\ \mu\text{m}$ radius) in olivine $\text{Fo}_{94.0}$ is shown in Table 3 (No. 13). Compositional profiles through the host olivine around this inclusion are shown in Fig. 6d. Diffusion profiles have been analysed around three melt inclusions in different high-Fo olivines, and all of them have similar shapes. The complete dataset is available from the first author.

The composition of the pillow-rim glass of this sample is shown in Table 3 (No. 14). This composition, which also contains 1 wt % H_2O (Sobolev & Danyushevsky, 1994), can be used to estimate the eruption temperature. The olivine liquidus temperature of this composition, 1060°C , calculated accounting for H_2O in the melt, represents the low-temperature end of the cooling interval. The residual melt inside the inclusion has a higher MgO content than the pillow-rim glass because the inclusion has a higher H_2O content (3.5 wt %, Sobolev & Danyushevsky, 1994). The calculated composition of the residual melt inside the inclusion at the moment of eruption is shown in Table 3 (No. 15). This residual melt has a lower FeO* content than the pillow-rim glass, a result of re-equilibration with the host evidenced by the diffusion profiles (Fig. 6d).

The initial trapped composition of this inclusion has been estimated by Sobolev & Danyushevsky (1994), and is shown in Table 3 (No. 16). This melt contained 2 wt % H_2O and had a liquidus temperature of $\sim 1380^\circ\text{C}$. Thus, the cooling interval of inclusion 5-25/OL3 was $\sim 320^\circ\text{C}$. The calculated compositions of the residual melt inside the inclusion at 0% and 100% re-equilibration after cooling over 320°C are shown in Table 3 (Nos 17 and 18).

The calculated diffusion profile for 86% re-equilibration in the case of instant cooling over 320°C is shown in Fig. 6d. This degree of re-equilibration will be achieved in ~ 150 days. The calculated profile matches well the observed compositional gradient. The calculated composition of the residual melt inside the inclusion at 86% re-equilibration (Table 3, No. 19) is also similar to the observed composition (Table 3, No. 15). The same degree of re-equilibration will be achieved in the case of cooling at a rate of 4°/day; however, the calculated profile does not match the data, and thus we conclude that in this case re-equilibration occurred while the grain was residing at $\sim 1060^\circ\text{C}$ before eruption.

DISCUSSION

Residence time of high-Fo olivine phenocrysts in mantle-derived magmas

In four samples described in the previous section, melt inclusions in high-Fo olivines suffered variable degrees of re-equilibration with their hosts, but none of them are completely re-equilibrated. Partially re-equilibrated melt inclusions in high-Fo olivines, i.e. inclusions that experienced moderate Fe-loss, have also been described in mid-ocean ridge basalt (MORB) samples from the Australia–Antarctic Discordance (Sigurdsson, 1994), Ocean Drilling Program (ODP) Hole 896A (McNeill, 1997), Macquarie Island (Kamenetsky *et al.*, 2000), Mid-Atlantic Ridge at 43°N and Bouvet Triple Junction (Kamenetsky *et al.*, 1998; V. S. Kamenetsky, personal communication, 2001); in subduction-related suites from the Troodos Ophiolite (Sobolev *et al.*, 1993; Portnyagin *et al.*, 1997), Kamchatka (Kamenetsky *et al.*, 1995b), Vanuatu and Sunda Arc (Danyushevsky *et al.*, 2000), Lau Basin (Kamenetsky *et al.*, 1997) and Roman Province in Italy (Kamenetsky *et al.*, 1995a; Marianelli *et al.*, 1999); in Icelandic picrites (Gurenko *et al.*, 1988, 1992; Gaetani & Watson, 2000); in primitive samples from Etna (Kamenetsky & Clocchiatti, 1996); and in Hawaiian samples (Sobolev & Nikogosian, 1994; Kent *et al.*, 1999; Sobolev *et al.*, 2000).

The only documented case of nearly complete re-equilibration of melt inclusions in high-Fo olivines is from the Ulakan Formation, Sunda Arc (Danyushevsky *et al.*, 2000), and we thus conclude that partial re-equilibration is a typical feature of melt inclusions in high-Fo olivine phenocrysts in mantle-derived magmas.

As follows from our analysis, partial re-equilibration of up to 80% is achieved within $\sim 10\%$ of the time required for complete re-equilibration. Assuming common sizes of melt inclusions (i.e. $<70\ \mu\text{m}$ in radius) and eruption temperatures of high-Fo olivine-bearing magmas of 1000°C or higher (e.g. Cas & Wright, 1987), it then follows that high-Fo phenocrysts usually spend

less than 3–5 months at temperatures between trapping and diffusion closure [Fig. 4, equation (1)].

This is not to say that high-Fo olivine phenocrysts do not reside in magma chambers for longer times. However, an apparent conclusion from our results is that if eruption does not happen within a few months after a primitive magma starts cooling and crystallization begins, olivines that crystallize from it are unlikely to be erupted as phenocrysts. A possible reason is that olivines quickly become separated from the melt and incorporated into the cumulate layer of the chamber.

This could explain the rarity of erupted high-Fo olivine-phyric rocks in well-developed island arcs (e.g. Marianas) and their common occurrence in more tectonically active arcs (e.g. SW Pacific, Smith *et al.* 1997). Indeed, if batches of primitive magma are not sufficiently large to cause an eruption of a magma chamber evolved under a mature volcano over many hundreds of thousands of years, then high-Fo olivines will end up ‘hidden’ in the cumulates under the volcano. This also explains why in mature island arcs olivine-phyric rocks are more common on small side-cones on the margins of large volcanoes (e.g. Graham & Hackett, 1987).

The residence times of erupted high-Fo olivine phenocrysts we calculate correspond to cooling rates faster than 1–2°/day. Such rates are consistent with results obtained from modelling of crystallization processes (e.g. Huppert & Sparks, 1980), which demonstrate that the cooling rates of primitive magmas are expected to vary between 1°/h and several degrees per day.

Gaetani & Watson (2000) have demonstrated that at cooling rates of 1–2°/year, olivine phenocrysts of commonly observed sizes will re-equilibrate with the surrounding magma, leading to irreversible changes in compositions of melt inclusions inside them. Our results demonstrate that such slow cooling rates are not appropriate for the cases when high-Fo olivine phenocrysts are erupted, and that olivines are efficiently separated from the parent magma, making their re-equilibration unlikely at any cooling rate. Thus, our results imply that erupted high-Fo olivine phenocrysts retain their original composition, and that compositions of melt inclusions in erupted high-Fo olivine phenocrysts *do not* suffer changes that cannot be reversed.

We also note that Gaetani & Watson (2000) have incorrectly restored the trapped composition of melt inclusions in high-Fo olivine phenocrysts from Icelandic picrites described in their paper. They did not take ‘Fe-loss’ into account and simply ‘added’ olivine to the partially re-equilibrated residual melt until it is in equilibrium with the host. This resulted in an artificially low FeO* content of the estimated trapped melt [see discussion by Danyushevsky *et al.* (2000)], and in their inability to reproduce the observed residual melt in the inclusions during modelling of post-entrapment changes

of the inclusion composition. Had the initial trapped composition been correctly estimated, their modelling would have reproduced the observed residual melt composition. Their suggestion that there existed 'an indeterminate period of slow cooling . . . , during which the host olivine maintained a close approach to Fe-Mg exchange equilibrium with both the magma and the inclusion' (Gaetani & Watson, 2000, p. 35) is entirely hypothetical and is not supported by observations.

Implications for the origin of high-Fo olivine-phyric volcanic rocks

Common features of high-Fo olivine-phyric samples include: (1) large, essentially unzoned cores of olivine phenocrysts; (2) a wide range (up to 15 Fo units) of phenocryst core compositions; (3) lack of correlation between the maximum Fo and rock MgO content within a cogenetic series; (4) evolved compositions of groundmass, which are often more evolved than what is expected to be in equilibrium with the least magnesian olivine phenocrysts (e.g. Falloon *et al.*, 1989; Gasparon, 1993; Sigurdsson *et al.*, 1993; Sobolev *et al.*, 1993; Sobolev & Nikogosian, 1994; Danyushevsky *et al.*, 1995; Kamenetsky *et al.*, 1995b, 1997; Marsh, 1996; McNeill & Danyushevsky, 1996; Della-Pasqua & Varne, 1997; Portnyagin *et al.*, 1997; see also a summary by Eggins, 1993, and their table 10).

Short residence times (or fast cooling rates) of high-Fo phenocrysts suggested by our results imply that the unzoned cores cannot reflect diffusive re-equilibration of originally zoned phenocrysts, as often assumed, but instead they are the result of fast efficient separation of olivines from the crystallizing magma. In other words, olivines are separated from the magma faster than melt changes its composition, and thus olivines and their parent magma cool separately. Such efficient separation is assisted by the low viscosity of primitive mantle-derived magmas; a large density contrast between olivines and mantle-derived melts; and the intensive convection that the primitive magmas are expected to experience during cooling (e.g. Huppert & Sparks, 1980). Because the surroundings of a crystallizing primitive magma are expected to be significantly cooler than the magma itself, separated olivine crystals should experience faster cooling rates than their parent magma. This suggests that the olivine rim on the walls of melt inclusions may grow rapidly, and that most re-equilibration with the host may occur during residence at the low-temperature end of the cooling interval (Fig. 1). Thus variations in residence time may in many cases be a more appropriate way to explain different degrees of re-equilibration of melt inclusions than variations in cooling rates.

It follows from the above arguments that the main source of high-Fo crystals in erupted magmas is the

cumulate zone. In other words, olivine-phyric rocks represent mixtures of an evolved transporting melt or magma (which forms the groundmass of the rock) with crystals that were formed during crystallization of more primitive melt(s). Such a mixed magma is formed during the eruption event and, as we discussed in the previous section, it is only possible when eruption occurs soon (within 3–5 months) after a new batch of primitive magma enters the magmatic system. The evolved magma, on the other hand, may reside in the chamber for a long time. This reconciles long magma residence times estimated from the compositions of rocks with short residence times of high-Fo olivine phenocrysts.

The variable distribution of phenocrysts in such mixed magmas will result in variably phyric rocks. In some suites, accumulated phenocrysts can locally constitute up to 50% of the mixture, leading to extremely high MgO contents in the rocks. For example, samples with >25 wt % MgO were described among Victorian boninites (Crawford, 1980), Siberian meimechites (Sobolev & Slutskiy, 1984), Troodos upper pillow lavas (Sobolev *et al.*, 1993), Tongan high-Ca boninites (Sobolev & Danyushevsky, 1994), Cape Vogel low-Ca boninites (Walker & Cameron, 1983), high-K arc suites from the Solomon Islands and Kamchatka (Ramsay *et al.*, 1984; Kamenetsky *et al.*, 1995b) and Hawaiian tholeiites (Sobolev & Nikogosian, 1994). The mixed origin of olivine-phyric rocks also explains the commonly observed coexistence in subduction-related volcanic rocks of unzoned high-Fo phenocrysts, incorporated from the cumulate zone, with substantially more evolved phenocrysts (low-magnesian pyroxenes and plagioclase) crystallized from the evolved transporting magma (e.g. Monzier *et al.*, 1993; Danyushevsky *et al.*, 1997).

Another confirmation of the mixed origin of high-Fo olivine-phyric rocks comes from observations of variably re-equilibrated melt inclusions of similar sizes occurring in a single sample in different olivine phenocrysts of a similar composition (Danyushevsky *et al.*, 2000). Similar compositions of host olivine imply similar cooling intervals, and thus variable degrees of re-equilibration are a result of either variable cooling rates experienced by individual phenocrysts, or variable residence time at a common temperature. This suggests that phenocrysts in these rocks must have come from different parts of the magmatic system. Marsh (1996, 1998) developed a plumbing system model that involves magma passing through a sequence of interconnected sills or chambers with a well-developed mush column. This column consists of a variety of local crystallization environments characterized by contrasting time scales of cooling. During an eruption, magma rising through such a column can inherit crystals from different pockets, and melt inclusions within these accumulated phenocrysts may be variably re-equilibrated.

A further implication from the mixed origin of olivine-phyric samples is that the compositional range of high-Fo olivine phenocrysts and their abundance are (1) a random result of the eruption process, and (2) usually non-representative of the crystallization history of the magma. Moreover, when compositionally different magma types erupt within a small spatial and temporal interval, the phenocrysts in rocks generated in the eruption of one magma type may have formed during the crystallization of another. Thus, in settings with diverse contemporaneous magmatism, the genetic relationship between host rocks and their olivine phenocrysts should not be assumed *a priori*. Instead, as also stressed by Falloon *et al.* (1989), the possibility of this type of mixing must be considered when using mineralogy as a tool for reconstructing parental melt compositions. Examples of such mixed rocks are known from the northern Tonga and central Vanuatu arcs (Falloon *et al.*, 1989; L. V. Danyushevsky & V. S. Kamenetsky, unpublished data, 2000). Melt inclusion studies are a powerful tool for identifying this type of mixing.

CONCLUSIONS

(1) Melt inclusions in high-Fo olivine phenocrysts from mantle-derived magmas are typically partially re-equilibrated with their hosts at temperatures below trapping. The mechanism of re-equilibration involves diffusion of Fe from and Mg into the initial volume of the inclusion. Quenched diffusion profiles around partially re-equilibrated inclusions can be used to estimate the cooling history of olivine phenocrysts between temperatures of their crystallization and diffusion closure.

(2) The re-equilibration process is fast. Our analysis demonstrates that at a reasonable combination of factors such as (1) cooling interval before eruption (<350°C), (2) eruption temperatures (>1000°C) and (3) inclusion size (<70 µm in radius), partial re-equilibration of up to 85% occurs within 3–5 months, corresponding to cooling rates faster than 1–2°/day. Such cooling rates are consistent with results of modelling of crystallization processes of primitive magmas (e.g. Huppert & Sparks, 1980).

(3) Short residence times of high-Fo phenocrysts suggest that if eruption does not happen within a few months after a primitive magma begins cooling and crystallization, olivines that crystallize from it are unlikely to be erupted as phenocrysts. This can be explained by efficient separation of olivine crystals from the melt, and their rapid incorporation into the cumulate zone. These results also suggest that in most cases erupted high-Fo olivine phenocrysts retain their original composition, and thus compositions of melt inclusions in erupted high-Fo olivine phenocrysts do not suffer changes that cannot be

reversed, contrary to the suggestion by Gaetani & Watson (2000).

(4) Short residence times of high-Fo phenocrysts, which commonly have large unzoned cores, imply that these cores cannot reflect diffusive re-equilibration of originally zoned phenocrysts. The unzoned cores are a result of fast efficient accumulation of olivines from the crystallizing magma, i.e. olivines are separated from the magma faster than melt changes its composition.

(5) The main source of high-Fo crystals in erupted magmas is the cumulate layers of the magmatic system. In other words, olivine-phyric rocks represent mixtures of an evolved transporting magma (which forms the groundmass of the rock) with crystals that were formed during crystallization of more primitive melt(s). Unlike high-Fo olivine phenocrysts, the evolved magma may reside in the magmatic system for a long time. This reconciles long magma residence times estimated from the compositions of rocks with short residence times of high-Fo olivine phenocrysts.

ACKNOWLEDGEMENTS

This research was supported by the Australian Research Council through QEII Research Fellowship and Research Grants to L.V.D. We wish to thank Dima Kamenetsky for critical comments on an earlier version of the paper. Formal reviews by Claude Herzberg and Chris Ballhaus have improved the original manuscript. We acknowledge support of the Museum of Natural History, Washington DC, which provided electron microprobe standards.

REFERENCES

- Albarède, F. (1993). Residence time analysis of geochemical fluctuations in volcanic series. *Geochimica et Cosmochimica Acta* **57**, 615–621.
- Ariskin, A. A. (1999). Phase equilibria modeling in igneous petrology: use of COMAGMAT model for simulating fractionation of ferro-basaltic magmas and the genesis of high-alumina basalt. *Journal of Volcanology and Geothermal Research* **90**, 115–162.
- Cas, R. A. F. & Wright, J. V. (1987). *Volcanic Successions, Modern and Ancient*. London: Allen & Unwin.
- Chakraborty, S. (1997). Rates and mechanisms of Fe–Mg interdiffusion in olivine at 980–1300°C. *Journal of Geophysical Research* **102B**, 12317–12331.
- Christensen, J. N. & DePaolo, D. J. (1993). Time scales of large volume silicic magma systems: Sr isotopic systematics of phenocrysts and glass from the Bishop Tuff, Long Valley, California. *Contributions to Mineralogy and Petrology* **113**, 100–114.
- Crawford, A. J. (1980). A clinoenstatite-bearing cumulate olivine pyroxenite from Howqua, Victoria. *Contributions to Mineralogy and Petrology* **75**, 353–367.
- Danyushevsky, L. V., Sobolev, A. V. & Falloon, T. J. (1995). North Tongan high-Ca boninite petrogenesis: the role of Samoan plume

- and subduction zone–transform fault transition. *Journal of Geodynamics* **20**, 219–241.
- Danyushevsky, L. V., Carroll, M. R. & Falloon, T. J. (1997). Origin of high-An plagioclase in Tongan high-Ca boninites: implications for plagioclase–melt equilibria at low $P(\text{H}_2\text{O})$. *Canadian Mineralogist* **35**, 313–326.
- Danyushevsky, L. V., Della-Pasqua, F. N. & Sokolov, S. (2000). Re-equilibration of melt inclusions trapped by magnesian olivine phenocrysts from subduction-related magmas: petrological implications. *Contributions to Mineralogy and Petrology* **138**, 68–83.
- Danyushevsky, L. V., McNeill, A. W. & Sobolev, A. V. (2002). Experimental and petrological studies of melt inclusions in phenocrysts from mantle-derived magmas: an overview of techniques, advantages and complications. *Chemical Geology* **183**, 4–25.
- Della-Pasqua, F. N. & Varne, R. (1997). Primitive ankaramitic magmas in volcanic arcs: a melt inclusion approach. *Canadian Mineralogist* **35**, 291–312.
- Eggins, S. M. (1993). Origin and differentiation of picritic arc magmas, Ambae (Aoba), Vanuatu. *Contributions to Mineralogy and Petrology* **114**, 79–100.
- Falloon, T. J. & Crawford, A. J. (1991). The petrogenesis of high-calcium boninites from the north Tonga ridge. *Earth and Planetary Science Letters* **102**, 375–394.
- Falloon, T. J. & Danyushevsky, L. V. (2000). Melting of refractory mantle at 1.5, 2.0 and 2.5 GPa under H_2O -undersaturated conditions: implications for the petrogenesis of high-Ca boninites and the influence of subduction components on mantle melting. *Journal of Petrology* **41**, 257–283.
- Falloon, T. J., Green, D. H. & McCulloch, M. T. (1989). Petrogenesis of high-Mg and associated lavas from the north Tonga trench. In: Crawford, A. J. (ed.) *Boninites and Related Rocks*. London: Unwin & Hyman, 357–395.
- Falloon, T. J., Green, D. H., O'Neill, H. St. C. & Hibberson, W. O. (1997). Experimental tests of low degree peridotite partial melt compositions: implications for the nature of anhydrous near-solidus peridotite melts at 1 GPa. *Earth and Planetary Science Letters* **152**, 149–162.
- Ford, C. E., Russel, D. G., Craven, J. A. & Fisk, M. R. (1983). Olivine–liquid equilibria: temperature, pressure and composition dependence of the crystal/liquid cation partition coefficients for Mg, Fe^{2+} , Ca and Mn. *Journal of Petrology* **24**, 256–265.
- Francalanci, L., Tommasini, S., Cinticelli, S. & Davies, G. R. (1999). Sr isotope evidence for short magma residence time for the 20th century activity at Stromboli volcano, Italy. *Earth and Planetary Science Letters* **167**, 61–69.
- Gaetani, G. A. & Watson, E. B. (2000). Open system behavior of olivine-hosted melt inclusions. *Earth and Planetary Science Letters* **183**, 27–41.
- Gasparon, M. (1993). Origin and evolution of mafic volcanics of Sumatra (Indonesia): their mantle source, and roles of subducted oceanic sediments and crustal contamination. Ph.D. thesis, University of Tasmania, Hobart, 395 pp.
- Graham, I. J. & Hackett, W. R. (1987). Petrology of calc-alkaline lavas from Ruapehu volcano and related vents, Taupo Volcanic Zone, New Zealand. *Journal of Petrology* **28**, 531–567.
- Gurenko, A. A., Sobolev, A. V., Polyakov, A. I. & Kononkova, N. N. (1988). Primary melt of rift tholeiites of Iceland: composition and conditions of crystallisation. *Transactions (Doklady) USSR Academy of Sciences* **301**(4), 109–113.
- Gurenko, A. A., Sobolev, A. V. & Kononkova, N. N. (1992). New petrological data on Icelandic rift alkali basalts. *Geochemistry International* **29**, 41–53.
- Hawkesworth, C. J., Blake, S., Evans, O., Hughes, R., Macdonald, R., Thomas, L. E., Turner, S. P. & Zellmer, G. (2000). Time scales of crystal fractionation in magma chambers—integrating physical, isotopic and geochemical perspectives. *Journal of Petrology* **41**, 991–1006.
- Huppert, H. E. & Sparks, R. S. J. (1980). The fluid dynamics of a basaltic magma chamber replenished by influx of hot, dense ultrabasic magma. *Contributions to Mineralogy and Petrology* **75**, 279–289.
- Kamenetsky, V. S. & Clocchiatti, R. (1996). Primitive magmatism of Mt. Etna: insights from mineralogy and melt inclusions. *Earth and Planetary Science Letters* **142**, 553–572.
- Kamenetsky, V. S., Metrich, N. & Cioni, R. (1995a). Potassic primary melts of Vulcini (Roman Province): evidence from mineralogy and melt inclusions. *Contributions to Mineralogy and Petrology* **120**, 186–196.
- Kamenetsky, V. S., Sobolev, A. V., Joron, J.-L. & Semet, M. P. (1995b). Petrology and geochemistry of Cretaceous Ultramafic Volcanics from Eastern Kamchatka. *Journal of Petrology* **36**, 637–662.
- Kamenetsky, V. S., Crawford, A. J., Eggins, S. & Muhe, R. (1997). Phenocryst and melt inclusion chemistry of near-axis seamounts, Valu Fa Ridge, Lau Basin: insight into mantle wedge melting and addition of subduction components. *Earth and Planetary Science Letters* **151**, 205–223.
- Kamenetsky, V. S., Eggins, S. M., Crawford, A. J., Green, D. H., Gasparon, M. & Falloon, T. J., (1998). Calcic melt inclusions in primitive olivine at 43°N MAR: evidence for melt–rock reaction/melting involving clinopyroxene-rich lithologies during MORB generation. *Earth and Planetary Science Letters* **160**, 115–132.
- Kamenetsky, V. S., Everard, J. L., Crawford, A. J., Varne, R., Eggins, S. M. & Lanyon, R. (2000). Enriched end-member of primitive MORB melts: petrology and geochemistry of glasses from Macquarie Island (SW Pacific). *Journal of Petrology* **41**, 411–430.
- Kent, A. J. R., Norman, M. D., Hutcheon, I. D. & Stolper, E. M. (1999). Assimilation of seawater-derived components in an oceanic volcano: evidence from matrix glasses and glass inclusions from Loihi seamount, Hawaii. *Chemical Geology* **156**, 299–319.
- Mangan, M. T. (1990). Crystal size distribution systematics and the determination of magma storage times: the 1959 eruption of Kilauea volcano, Hawaii. *Journal of Volcanology and Geothermal Research* **44**, 295–302.
- Marianelli, P., Métrich, N. & Sbrana, A. (1999). Shallow and deep reservoirs involved in magma supply of the 1944 eruption of Vesuvius. *Bulletin of Volcanology* **61**, 48–63.
- Marsh, B. D. (1996). Solidification fronts and magmatic evolution. *Mineralogical Magazine* **60**, 5–40.
- Marsh, B. D. (1998). On the interpretation of crystal size distribution in magmatic systems. *Journal of Petrology* **39**, 553–599.
- McNeill, A. W. (1997). The crystallisation history of normal mid-ocean ridge basalts from the eastern Pacific Ocean and implications for the composition of primary mid-ocean ridge magmas: evidence from mineralogy, pillow-rim glasses and melt inclusion studies. Ph.D. thesis, University of Tasmania, Hobart, 258 pp.
- McNeill, A. W. & Danyushevsky, L.V. (1996). Compositions and crystallization temperatures of primary melts for Hole 896A basalts: evidence from melt inclusion studies. In: Alt, J. C., Kinoshita, H., Stokking, L. B. & Michael, P. J. (eds) *Proceedings of the Ocean Drilling Program, Scientific Results, 148*. College Station, TX: Ocean Drilling Program, pp. 21–35.
- Monzier, M., Danyushevsky, L. V., Crawford, A. J., Bellon, H. & Cotton, J. (1993). High-Mg andesites from the southern termination of the New Hebrides island arc (SW Pacific). *Journal of Volcanology and Geothermal Research* **57**, 193–217.
- Nakamura, M. (1995). Residence time and crystallization history of nickeliferous olivine phenocrysts from the northern Yatsugatake

- volcanoes, Central Japan: application of a growth and diffusion model in the system Mg–Fe–Ni. *Journal of Volcanology and Geothermal Research* **66**, 81–100.
- Nisbet, E. G., Arndt, N. T., Bickle, M. J., Cameron, W. E., Chauvel, C., Cheadle, M. J., Hegner, E., Kyser, T. K., Martin, A., Renner, R. & Roedder, E. (1987). Uniquely fresh 2.7 Ga komatiites from the Belingwe greenstone belt, Zimbabwe. *Geology* **15**, 1147–1150.
- Perfit, M. R., Fornari, D., Ridley, W. I., Kirk, P. D., Casey, J. F., Kastens, K. A., Reynolds, J. R., Edwards, M., Desonie, D., Shuster, R. & Paradis, S. (1996). Recent volcanism in the Siqueiros transform fault: picritic basalts and implications for MORB magma genesis. *Earth and Planetary Science Letters* **141**, 91–108.
- Portnyagin, M. V., Danyushevsky, L. V. & Kamenetsky, V. S. (1997). Coexistence of two distinct mantle sources during formation of ophiolites: a case study of primitive pillow-lavas from the lowest part of the volcanic section of the Troodos Ophiolite, Cyprus. *Contributions to Mineralogy and Petrology* **128**, 287–301.
- Pyle, D. M. (1992). The volume and residence time of magma beneath active volcanoes determined by decay-series disequilibria methods. *Earth and Planetary Science Letters* **112**, 61–73.
- Ramsay, W. R. H., Crawford, A. J. & Foden, J. D. (1984). Field setting, mineralogy, chemistry and genesis of arc picrites, New Georgia, Solomon Islands. *Contributions to Mineralogy and Petrology* **88**, 386–402.
- Renner, R., Nisbet, E. G., Cheadle, M. J., Arndt, N. T., Bickle, M. J. & Cameron, W. E. (1994). Komatiite flows from the Reliance Formation, Belingwe Belt, Zimbabwe: I. Petrography and mineralogy. *Journal of Petrology* **35**, 361–400.
- Sigmarrsson, O. (1996). Short magma chamber residence time at an Icelandic volcano inferred from U-series disequilibria. *Nature* **382**, 440–442.
- Sigurdsson, I. A. (1994). Primitive magmas in convergent margins and at oceanic spreading ridges: evidence from early formed phenocryst phases and their melt inclusions. Ph.D. thesis, University of Tasmania, Hobart, 243 pp.
- Sigurdsson, I. A., Kamenetsky, V. S., Crawford, A. J., Eggins, S. M. & Zlobin, S. K. (1993). Primitive island arc and oceanic lavas from the Hunter ridge–Hunter fracture zone. Evidence from glass, olivine and spinel compositions. *Mineralogy and Petrology* **47**, 149–169.
- Smith, I. E. M., Worthington, T. J., Price, R. C. & Gamble, J. A. (1997). Primitive magmas in arc-type volcanic associations: examples from the Southwest Pacific. *Canadian Mineralogist* **35**, 257–273.
- Sobolev, A. V. & Chaussidon, M. (1996). H₂O concentrations in primary melts from island arcs and mid-ocean ridges: implications for H₂O storage and recycling in the mantle. *Earth and Planetary Science Letters* **137**, 45–55.
- Sobolev, A. V. & Danyushevsky, L. V. (1994). Petrology and geochemistry of boninites from the north termination of the Tonga Trench: constraints on the generation conditions of primary high-Ca boninite magmas. *Journal of Petrology* **35**, 1183–1211.
- Sobolev, A. V., Hofmann, A. W. & Nikogosian, I. K. (2000). Recycled oceanic crust observed in ‘ghost plagioclase’ within the source of Mauna Loa lavas. *Nature* **404**, 986–990.
- Sobolev, A. V. & Nikogosian, I. K. (1994). Petrology of long-lived mantle plume magmatism: Hawaii, Pacific, and Reunion Island, Indian Ocean. *Petrology* **2**, 111–144.
- Sobolev, A. V., Portnyagin, M. V., Dmitriev, L. V., Tsamerian, O. P., Danyushevsky, L. V., Kononkova, N. N., Shimizu, N. & Robinson, P. T. (1993). Petrology of ultramafic lavas and associated rocks of the Troodos Massif, Cyprus. *Petrology* **1**, 331–361.
- Sobolev, A. V. & Slutskiy, A. B. (1984). Composition and crystallisation conditions of the initial melt of the Siberian meimechites in relation to the general problem of the ultrabasic magmas. *Soviet Geology and Geophysics* **25**, 93–104.
- Ulmer, P. (1989). The dependence of the Fe²⁺–Mg cation-partitioning between olivine and basaltic liquid on pressure, temperature and composition. An experimental study to 30 kbar. *Contributions to Mineralogy and Petrology* **101**, 261–273.
- Volpe, A. M. & Hammond, P. E. (1991). ²³⁰U–²³⁰Th–²²⁶Ra disequilibria in young Mount St. Helens rocks: time constraint for magma formation and crystallisation. *Earth and Planetary Science Letters* **107**, 475–486.
- Walker, D. A. & Cameron, W. E. (1983). Boninite primary magmas: evidence from the Cape Vogel peninsula, PNG. *Contributions to Mineralogy and Petrology* **83**, 150–158.
- Zellmer, G. F., Blake, S., Vance, D., Hawkesworth, C. & Turner, S. (1999). Plagioclase residence times at two island arc volcanoes (Kameni Islands, Santorini, and Soufriere, St. Vincent) determined by Sr diffusion systematics. *Contributions to Mineralogy and Petrology* **136**, 345–357.